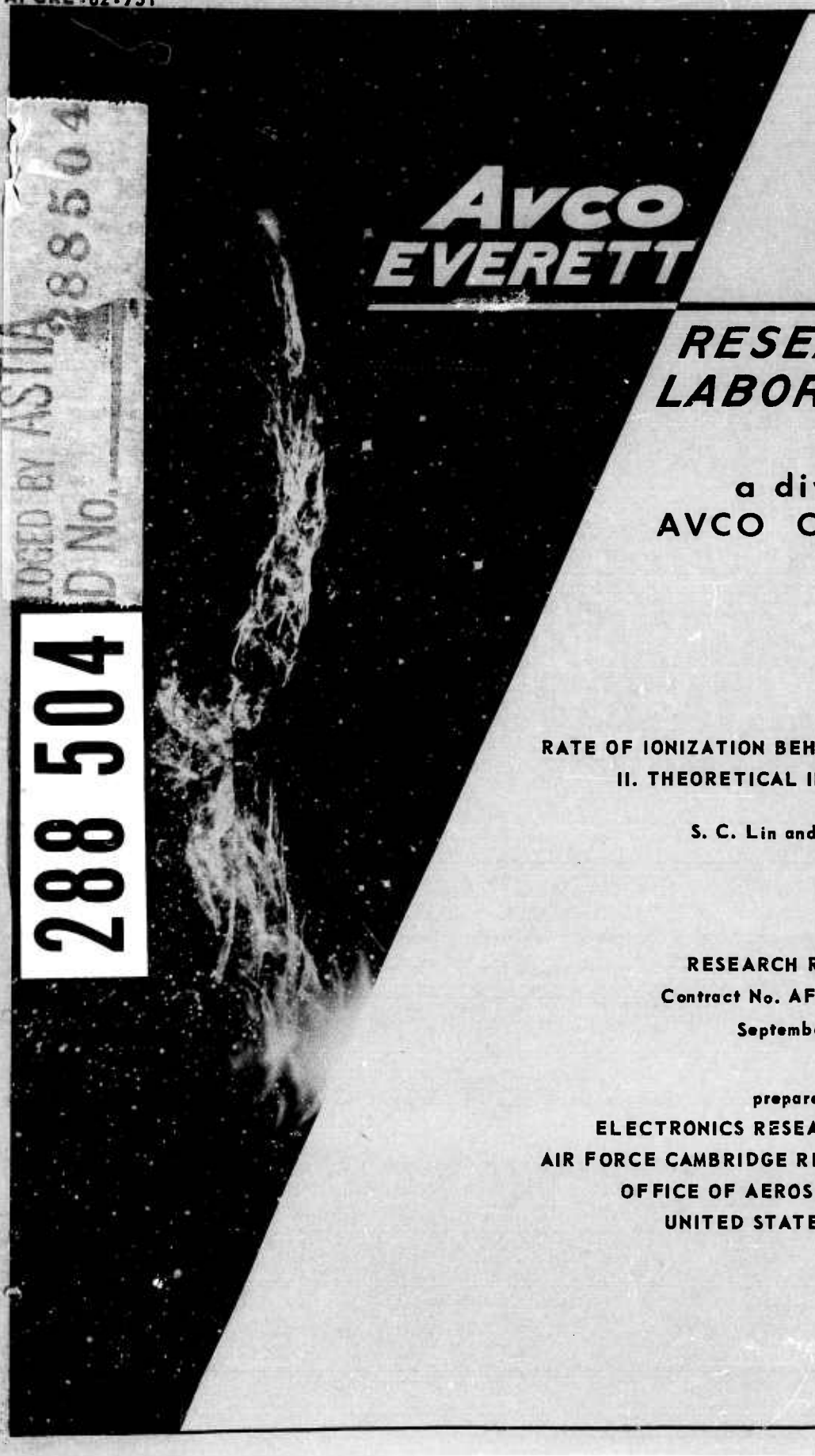

AVCO EVERETT RESEARCH LABORATORY

a division of
AVCO CORPORATION

RATE OF IONIZATION BEHIND SHOCK WAVES IN AIR
II. THEORETICAL INTERPRETATION

S. C. Lin and J. D. Teare

RESEARCH REPORT 115
Contract No. AF 19(604)-7458
September 1962

prepared for
ELECTRONICS RESEARCH DIRECTORATE
AIR FORCE CAMBRIDGE RESEARCH LABORATORIES
OFFICE OF AEROSPACE RESEARCH
UNITED STATES AIR FORCE

AFCRL-62-751 RESEARCH REPORT 115

RATE OF IONIZATION BEHIND SHOCK WAVES IN AIR
II. THEORETICAL INTERPRETATION

by

S. C. Lin and J. D. Teare

AVCO-EVERETT RESEARCH LABORATORY
a division of
AVCO CORPORATION
Everett, Massachusetts

Contract No. AF 19(604)-7458

Project 5561
Task 46308

September 1962

prepared for

ELECTRONICS RESEARCH DIRECTORATE
AIR FORCE CAMBRIDGE RESEARCH LABORATORIES
OFFICE OF AEROSPACE RESEARCH
UNITED STATES AIR FORCE
Bedford, Massachusetts

ABSTRACT

The problem of spontaneous ionization (i. e., no externally applied electromagnetic fields, nor hard radiation) in the reaction zone behind strong normal shock waves in air has been treated concurrently with the problem of dissociation and vibrational relaxation. Through a comparison of specific ionization rates, one may conclude that up to a shock velocity of 10 km/sec (about 30 times the speed of sound at room temperature) the predominant electron production process would be atom-atom ionizing collisions. This would be followed in an approximately decreasing order of importance by photoionization, electron impact, atom-molecule collisions and molecule-molecule collisions. The charge exchange reactions, while not contributing directly to the electron production process, were found to have a small but noticeable indirect effect on the resultant electron density distribution at some distance behind the shock due to their continuous shifting of the relative population between atomic and molecular ions (which recombine with the electrons at different rates). The specific rate constants for the atom-atom processes required to interpret all existing experimental results appear to be consistent with a simple extrapolation of the low temperature rate constants according to the crossing-point model of Bates and Massey for atom-atom ionizing collisions.

I. INTRODUCTION

In a complementary paper, Lin, Neal and Fyfe[1] have presented experimental results showing some typical electron density profiles behind normal shock waves in air at initial pressure $0.02 \leq p_1 \leq 0.2$ mm Hg. and in the shock velocity range $4.5 \leq U_s \leq 7$ km/sec (or shock Mach number range $14 \leq M_s \leq 20$). They have also presented various measured quantities which may be used to characterize the ionization history behind the shock front. The essential result was that within the range of shock strength covered, the characteristic ionization distance was only about 10 to 40 times the viscosity mean free path of the undisturbed gas ahead of the shock, and that the electron density appeared to "overshoot" the equilibrium value by a considerable factor for some distance behind the shock front before relaxing back toward the final equilibrium value.

The problem of approach to equilibrium ionization behind strong shock waves in argon has been extensively treated by Petschek and Byron,[2] and also by Bond.[3] The general conclusion was that the main part of the ionization history was dominated by the electron impact process, even though the starting mechanism which accounted for about 10 percent of the total ionization was not clear. The local ionization rate at any point within the main ionization zone was then completely determined by the local degree of ionization (i.e., fraction of atoms ionized) and the electron temperature. The electron temperature was determined by a balance between the rate at which electrons lose energy in the ionizing collisions and the rate at which they regain energy from elastic collisions with the hotter positive ions and the neutral atoms. The translational temperature of the latter was, in turn, uniquely determined by the local degree of ionization and the energy equation.[2] The resultant effect was that the electron density increased monotonically in an approximately exponential manner until the backward rate (i.e., electron-ion recombination) became sufficiently rapid to limit the net rate of electron production.

While the approach to ionization equilibrium behind extremely strong shock waves in air (i.e., kinetic energy per air molecule much greater than the dissociation energy) may assume some of the characteristics of

the argon shock just described, the predominant ionization path is likely to be very different at more moderate shock velocities where the dissociation energy remains an important part of the total energy storage behind the shock. The presence of more than one chemical species in the initial gas mixture is also expected to further complicate the air problem.

Results obtained from studies of relaxation phenomena in air and its component gases have been reported by the authors and their colleagues on various occasions over the past years.[4-7] These studies have included critical examination of the steadily growing volume of chemical kinetic data, but the ionization processes have only been treated in a cursory manner.

In the present paper, the various ionization processes that may play significant roles behind strong shock waves in air will be critically examined. The composite ionization history behind the shock will be constructed from these processes along with the chemical and vibrational relaxation processes for various shock conditions. The theoretical results will then be used to interpret the experimental results reported in the complementary paper.[1] Some remarks will also be made concerning the validity of extrapolating the present theoretical model to a wider range of shock conditions.

II. COUPLING BETWEEN VIBRATIONAL EXCITATION, DISSOCIATION AND IONIZATION

It is well known that the combined problem of vibrational and radiative excitations, dissociation, and ionization behind strong shock waves in a diatomic gas mixture, such as air, is very complex on account of the large number of species and reactions which must be simultaneously considered and followed.[8,9] However, in a situation where the degree of ionization remains sufficiently low and the radiative heat loss is small compared with the rate of enthalpy flow across the shock front, one may take advantage of the "one-way coupling" between the dissociation process and the ionization and radiative excitation processes. In other words, while the local ionization and radiative excitation rates at any given point behind the shock front are sensitive to the local temperature and chemical composition resulting from the vibrational excitation and molecular reactions, they do not contribute significantly to the reaction rates of these molecular processes, nor do they affect the energy balance in a significant manner. In such a

situation, one may first determine the temperature, density, and chemical composition profiles independent of the ionization and photo processes. From these, one can then calculate the ionization and radiation profiles from the corresponding specific rates for these processes. However, at higher shock strengths, such an iterative procedure would not be satisfactory, and one must consider the electronic and photo processes simultaneously with the chemical processes in the shock profile determination. For the case of air, the dividing point for the two situations should be somewhere about 10 km/sec shock velocity, where the maximum degree of ionization behind the shock does not appreciably exceed one percent.

In the present paper, we shall consider only the simpler situation in which the coupling between dissociation and ionization is approximately one way. Then, considering air to be an initially binary mixture consisting of 21% O_2 and 79% N_2 by partial pressure (inclusion of argon, CO_2, H_2O and other minor constituents would only complicate the computational work without contributing to the essential results), one may proceed to determine the temperature, density, molecular and atomic concentration profiles behind the shock from the following major chemical reactions:

$$O_2 + X + 5.1\ \text{e.v.} \rightleftharpoons O + O + X \qquad (1)$$

$$N_2 + X + 9.8\ \text{e.v.} \rightleftharpoons N + N + X \qquad (2)$$

$$NO + X + 6.5\ \text{e.v.} \rightleftharpoons N + O + X \qquad (3)$$

$$O + N_2 + 3.3\ \text{e.v.} \rightleftharpoons NO + N \qquad (4)$$

$$N + O_2 - 1.4\ \text{e.v.} \rightleftharpoons NO + O \qquad (5)$$

$$N_2 + O_2 + 1.9\ \text{e.v.} \rightleftharpoons NO + NO \qquad (6)$$

The chemical symbols employed in the above expressions are conventional, except that we have used X to represent any molecule or atom in the dissociating gas mixture. The energy of reaction at $O^{\circ}K$ is given in electron-volts (e.v.). Reactions (1) through (5) are the same as those considered in

earlier works by the authors[4,6,8,10] and by others[9] in connection with the problems of chemical reactions behind shock waves and in the flow fields of high temperature air. The bimolecular reaction (6) was thought to be unimportant, but recent studies of the decomposition rate of NO behind shock waves by Freedman and Daiber[11] and by Wray and Teare[12] suggested that the rate constant for this reaction in the temperature range of interest could be much greater than what had been previously estimated.[13,14] This reaction has subsequently been included in more recent works.[15,17] It was found that this reaction does affect the initial rate of formation of NO behind the shock, but the overall effect on the ionization processes appears to be minor.

From the set of chemical reactions shown above, and from the usual definition of the constant-volume reaction rate constant κ_1^X, κ_{R1}^X (superscript referring to the catalyst X), etc., one may write for the total time rate of change of molecular oxygen number density following any fluid element,

$$\frac{d}{dt}(n_{O_2}) = n_{O_2}\frac{d\ln\rho}{dt} - \sum_X(\kappa_1^X n_{O_2} n_X - \kappa_{R1}^X n_O^2 n_X) - \kappa_5 n_N n_{O_2} + \kappa_{R5} n_{NO} n_O - \kappa_6 n_{N_2} n_{O_2} + \kappa_{R6} n_{NO}^2 \qquad (7)$$

Or, in terms of the normalized number density $[X] \equiv n_X/n_{air}$, where $n_{air} \equiv (\rho/\rho_1)\, n_1$ is the equivalent number of air molecules per unit volume at the local mass density ρ behind the shock, and n_1, ρ_1 denote, respectively, the initial number density and mass density ahead of the shock,

$$\frac{d[O_2]}{dt} = -\left(\sum_X \kappa_1^X [X] + \kappa_5 [N] + \kappa_6 [N_2]\right)[O_2] \frac{\rho}{\rho_1} n_1 + \left(\kappa_{R5} [NO][O] + \kappa_{R6} [NO]^2\right) \frac{\rho}{\rho_1} n_1 + \sum_X \kappa_{R1}^X [O]^2 [X] \left(\frac{\rho}{\rho_1}\right)^2 n_1^2 \quad (7\text{-a})$$

Similar equations can be written for the total time rate of change of the number density for other chemical species.

In addition to the chemical reactions listed above, one must also consider the effects of molecular vibrational relaxation, and of the coupling between vibrational relaxation and dissociation. As has been proposed by Hammerling, Teare and Kivel,[7] these effects can be approximately taken into account by applying a correction factor of the form

$$\eta = \frac{1 - \exp\left[-N_v (\Theta_v - \Theta)\right]}{N_v \left[\exp(\Theta_v - \Theta) - 1\right]} \cdot \frac{\exp \Theta_v - 1}{\exp \Theta - 1} \quad (8)$$

to the dissociation rate constant corresponding to local vibration-translation equilibrium $(\kappa^X)_{eq.}$, such that

$$\kappa^X = (\kappa^X)_{eq.} \cdot \eta \quad (9)$$

In Eq. (8), N_v denotes the total number of vibrational levels for the molecule considered (assuming N_v to be finite and the levels equally spaced); $\Theta_v \equiv E_v/kT_v$ and $\Theta \equiv E_v/kT$ are respectively the reciprocal of the vibrational and

translational temperature normalized with respect to the vibrational energy spacing E_v (k being the Boltzmann constant). The vibrational temperature is related to the translational temperature through the usual relaxation expression

$$\frac{d\mathcal{E}_v}{dt} = \frac{(\mathcal{E}_v)_{eq.} - \mathcal{E}_v}{\tau_v} \tag{10}$$

where $\mathcal{E}_v = E_v/(\exp \Theta_v - 1)$ is the mean vibrational energy per molecule; and τ_v is the vibrational relaxation time, which may be assumed to depend only on the translational temperature and particle density.[18,19]

The coupling mechanism between vibrational relaxation and dissociation discussed above is equivalent to assigning equal weight to the pre-exponential factor for the partial dissociation rate constant for the various vibrational states, and it assumes that the population of the vibrational states follows the Boltzmann distribution at all times throughout the relaxation process.[20]

The conservation equations for a plane shock wave propagating at a constant velocity U_s in an otherwise undisturbed atmosphere of density ρ_1 and pressure p_1 are given by (neglecting viscous dissipation within the reaction zone and radiative heat loss),[21]

Mass:
$$\rho u = \rho_1 U_s \tag{11}$$

Momentum:
$$p + \rho u^2 = p_1 + \rho_1 U_s^2 \tag{12}$$

$$\text{Energy:}\quad \frac{\varepsilon}{m} + \frac{p}{\rho} + \frac{u^2}{2} = \frac{\varepsilon_1}{m} + \frac{p_1}{\rho_1} + \frac{U_s^2}{2} \qquad (13)$$

where u is the local mass velocity in a coordinate system fixed to the propagating shock front, $p = kT \sum_X n_X$ is the local gas pressure, and

$$\varepsilon = \sum_X [X]\ \varepsilon_X \qquad (14)$$

is the total thermal and chemical energy per equivalent air molecule, and m is the mass per air molecule. Note that ε depends only on the local translational temperature T, the vibrational temperatures $(T_v)_{O_2}$, $(T_v)_{N_2}$, and the normalized particle densities $[X]$.

By integrating the chemical rate equations (of which Eq. (7) is a typical example) and the vibrational relaxation equations for O_2 and N_2 simultaneously under the constraints of these conservation equations, one can follow the translational and vibrational temperatures, mass density, and particle densities as a function of time t, or distance

$$x = \int_0^t u\,dt$$

behind the translational/rotational shock front for any given set of initial conditions. This is illustrated in Figs. 1(a), (b), (c) and 2 (a), (b), (c) where the local temperatures, mass density, and chemical composition behind a plane shock wave in air at three different velocities in the range of initial pressure $0.02 \leq p_1 \leq 2$ mm Hg are plotted as functions of the normalized distance behind the shock (i.e., normalized with respect to the upstream mean free path ℓ_1). The vibrational temperature for NO can be assumed to be identical to the translational temperature since this chemical species is produced only through energetic collisions behind the shock.

The method of solution and computational procedure employed in obtaining the numerical results presented here are essentially the same as those described in Ref. 12. It may be mentioned again that, as a simplifying approximation, vibrational relaxation and chemical reactions within the translational/

rotational relaxation zone have been completely neglected, so that the starting point x = O actually refers to some fictitious point at which the gas temperature and density assume values corresponding to full translational/rotational relaxation behind the shock. Since the actual characteristic distance for translational/rotational relaxation behind strong shock waves is known to be comparable to the upstream mean free path,[6,22] the physical meaning for the region $x/\ell_1 \leq 1$ in the present model becomes ambiguous. For the region $x/\ell_1 > 1$, there would also be an uncertainty of the order of unity in the absolute scale of x/ℓ_1 with respect to the center of the translational/rotational relaxation zone. These, however, may not be considered as serious limitations as long as the characteristic distances for vibrational relaxation and chemical reactions are still considerably greater than ℓ_1.

The chemical rate constants employed in the present calculations are summarized in Table I. Aside from the addition of the bimolecular reaction (6), this set of rate constants is essentially the same as those quoted in Refs. 4 and 6, with the exception of an upward revision of $\kappa_{R1}^{N_2}$, and κ_{R2}^{N}, by a factor of 2 and 4, respectively; a reassignment of the catalytic efficienty of O and N in reaction (3), and some minor adjustments of the temperature dependence for $\kappa_{R2}^{N_2}$ and κ_5 according to the recent review paper by Wray.* The equilibrium constants employed to relate the backward and forward rate constants for each reaction are based on standard spectroscopic data.[23-25]

The most striking features of the temperature and chemical composition profiles for strong shock waves in air as exhibited in Figs. 1 and 2 are perhaps the rapid progress of the oxygen-nitrogen reactions immediately behind the shock front on the one hand and the relatively long time it takes some of the reactions to approach the final adiabatic equilibrium state behind the shock on the other hand. For example, at a distance of 10 mean free paths behind the translational/rotational shock front for the median shock

*It may be mentioned that Wray in Ref. 15 has suggested adopting the same temperature dependence for all catalyst X in reaction (1). However, this would tend to overestimate the relative catalytic efficiencies for O and O_2 at high temperatures (i.e., $T > 8000^{\circ}K$). Therefore, the rate constants κ_{R1}^{O} and $\kappa_{R1}^{O_2}$ as quoted in Refs. 4 and 6 are still preferred.

TABLE I

Summary of chemical rate constants employed in neutral particle concentration determination (T in ^{o}K, concentration in particles/cm^3, time in seconds).

	RATE CONSTANT	CATALYST X
κ^{X}_{R1} =	$6.2 \times 10^{-28}\ T^{-3/2}$	O
	$2.2 \times 10^{-28}\ T^{-3/2}$	O_2
	$1.7 \times 10^{-32}\ T^{-1/2}$	N_2
	$8.3 \times 10^{-33}\ T^{-1/2}$	N, NO
κ^{X}_{R2} =	$6.5 \times 10^{-27}\ T^{-3/2}$	N
	$7.6 \times 10^{-32}\ T^{-1/2}$	N_2
	$3.0 \times 10^{-32}\ T^{-1/2}$	O_2, O, NO
κ^{X}_{R3} =	$5.5 \times 10^{-27}\ T^{-3/2}$	NO
	$2.8 \times 10^{-28}\ T^{-3/2}$	O, N, O_2, N_2
κ_{R4} =	2.7×10^{-11}	
κ_{5} =	$2.2 \times 10^{-14}\ T \exp(-3,560/T)$	
κ_{R6} =	$0.4\ T^{-5/2} \exp(-43,000/T)$	

velocity cited (i. e., U_s = 6.9 km/sec), dissociation of O_2 and N_2 have reached 75% and 50% of the final equilibrium level respectively, and the translational temperature has dropped by a factor of two from the initial value. On the other hand, it takes a distance of several hundred mean free paths (depending on the initial pressure p_1) in order for N_2 dissociation and the translational temperature to come within 10% of the final equilibrium level. The rapid initial rates of change in temperature and chemical composition imply that the various competing ionization processes may carry different weights at different distances behind the shock front. The long chemical relaxation time toward the equilibrium state implies that the degree of ionization may also be expected to depart from the final equilibrium level for a large distance behind the shock front.

Further discussion of the vibrational and chemical relaxation histories is beyond the scope of the present paper, but an illustration of how the various reactions proceed behind the shock front can be found in the recent paper by Wray.[15] Similar illustration can also be found in an earlier paper by Duff and Davidson,[9] in which substantially different rate constants were used for some of the important reactions. The effect of this different choice of the rate constants were discussed in Ref. 6.

III. THE COMPETING IONIZATION PROCESSES

To determine the ionization history behind the shock front in the energy range of interest (see preceding section) we shall consider the following classes of ionization processes:

Electron-Impact and Ion-Impact Ionization

$$e + X \rightleftharpoons X^+ + e + e \qquad (15)$$

$$X^+ + Y \rightleftharpoons X^+ + Y^+ + e \qquad (16)$$

Photoionization

$$h\nu + X \rightleftharpoons X^+ + e \qquad (17)$$

Charge Exchange

$$X^+ + Y \rightleftharpoons X + Y^+ \qquad (18\text{-a})$$

$$A^+ + B_2 \rightleftharpoons AB + B^+ \qquad (18\text{-b})$$

$$X^+ + Y \rightleftharpoons X + Y^{++} + e \qquad (18\text{-c})$$

Electron Attachment

$$e + X \rightleftharpoons X^- \qquad (19\text{-a})$$

$$e + X \rightleftharpoons X^- + h\nu \qquad (19\text{-b})$$

$$e + AB \rightleftharpoons A + B^- \qquad (19\text{-c})$$

Ionization by Neutral Atom and Molecule Collisions

$$X + Y \rightleftharpoons X^+ + Y + e \qquad (20)$$

$$A + B \rightleftharpoons AB^+ + e \qquad (21)$$

$$A + B_2 \rightleftharpoons AB_2^+ + e \qquad (22\text{-a})$$

$$A + B_2 \rightleftharpoons AB^+ + B + e \qquad (22\text{-b})$$

$$A_2 + B_2 \rightleftharpoons A_2B^+ + B + e \qquad (23\text{-a})$$

$$A_2 + B_2 \rightleftharpoons AB^+ + AB + e \qquad (23\text{-b})$$

In the above expressions, we have used the symbols, X, Y, to represent any neutral molecule or atom; the symbols A, B, to represent a neutral atom only (i. e., diatomic molecules to be represented by A_2, B_2, AB, etc.), and the symbol e to represent a free electron. The above list is selective rather than comprehensive, in the sense that only processes involving the lowest energies of reaction within each group have been included. We have also excluded electron production processes requiring 3-body collisions, since they would be relatively infrequent in the range of gas density under consideration. To avoid further complication by the question of distribution among the various vibrational and electronic states for the molecules, atoms, and ions involved in Eqs. (15) through (23-b), we shall henceforth regard all the cross-sections (or rate constants) associated with these electronic processes as averaged quantities over the appropriate internal energy states, unless otherwise noted.

In addition to the gas-phase reactions listed above, one may also consider various secondary processes, such as electron diffusion and photo-electric effects from solid surfaces, which have been observed in some noble gas experiments.[26,27] Since these effects are generally weak compared with the main ionization processes, and are to some extent geometry-dependent, we shall postpone our discussion of these effects until later in Section IV.

Let us consider now the various gas-phase ionization processes in some detail. In view of the fact that the forward and backward rates are closely related for each process through the local equilibrium constant, we only need to discuss either one of the two rates in each case.

A. Electron-Impact and Ion-Impact Ionization

Electron-impact ionization has long been known to be the single most important electron production process in almost every gas discharge phenomenon.[28,29] It has been found to be also the main ionization process behind strong shock waves in noble gases.[2,3]

In terms of the local electron energy distribution function $f(\epsilon)$, and the total ionization cross section $Q_{iX}(\epsilon)$ for collisions between electrons of energy ϵ and molecules or atoms of type X, the instantaneous rate of production of ion pairs per unit volume following a fluid element behind the shock front is given by (considering only the forward rate).[30]

$$\left(\frac{dn_e}{dt}\right)_{(15)} = n_e \sum_X n_X \int_{w_{iX}}^{\infty} v\, Q_{iX}(\epsilon) \cdot f(\epsilon)\, d\epsilon \qquad (24)$$

where n_e is the local number density of free electron; w_{iX} is the threshold energy for the ionization cross section Q_{iX}; $v = (2\epsilon/m_e)^{1/2}$ is the electron speed corresponding to energy ϵ (m_e being the electron mass).

In the absence of strong electromagnetic fields, the electron energy distribution will be approximately Maxwellian at a temperature T_e which is comparable, but not necessarily equal, to the local translational gas temperature T. Strictly speaking, the electron temperature profile behind the shock front should be determined from a detailed consideration of the local energy balance for the free electrons within each fluid element, taking into account the effect of heat conduction by the electrons (due to the high thermal conductivity of the electrons and the large variation in temperature within the reaction zone); as well as the effects of energy transfer between the heavier particles and the electrons; energy loss by the electrons in impact ionization and excitation, etc.[2] However, in view of the fact that energy

transfer for collisions between diatomic molecules and electrons appears to be quite efficient,* and that the electron mean free path is generally much smaller than the thickness of the reaction zone, the actual lag between the two temperatures may not be too great. Therefore, in a first approximation, we may consider T_e to be everywhere the same as T in estimating the impact ionization rate. Thus, Eq. (24) becomes

$$\left(\frac{dn_e}{dt}\right)_{(15)} \cong n_e \left(\frac{8}{\pi m_e}\right)^{1/2} \left(\frac{1}{kT}\right)^{3/2} \sum_X n_X \int_{w_{iX}}^{\infty} \exp\left(-\frac{\epsilon}{kT}\right) \cdot Q_{iX}(\epsilon)\, \epsilon\, d\epsilon \tag{25}$$

for $kT \ll w_{iX}$ the above equation may be approximated by its asymptotic equivalent,[31]

$$\left(\frac{dn_e}{dt}\right)_{(15)} \sim n_e \left(\frac{8kT}{\pi m_e}\right)^{1/2} \sum_X n_X \exp\left(-\frac{w_{iX}}{kT}\right) \cdot w_{iX} Q'_{iX}(w_{iX}) \tag{26}$$

where $Q'_{iX}(w_{iX})$ is the slope of the Q_{iX} vs ϵ curve at (or near) the threshold energy w_{iX}.

The ionization efficiencies by electron impact for N_2, O_2, and NO and a number of other molecular gases at room temperature have been measured by Tate and Smith.[32] The apparent ionization cross-section as deduced by Massey and Burhop** from these measurements is reproduced here in Fig. 3 for electron energies up to several times the threshold energy. It is seen that these cross-sections are all characterized by an approximately linear rise near the threshold, which continues on for a considerable distance

*See for example, Massey and Burhop, loc. cit., Table VI, p. 279.

**H. S. W. Massey and E. H. S. Burhop, loc. cit., Table III, p. 265.

beyond the threshold; a maximum value which is several times the atomic unit of area πa_o^2 (where $a_o = 5.29 \times 10^{-9}$ cm is the first Bohr radius) at about 100 e.v.; and then a gradual fall-off at higher electron energies. It may also be noted that the products $w_{iX}\bar{Q}'_{iX}$ (w_{iX}) for these molecules are all very nearly equal to πa_o^2.

For atomic oxygen O, and atomic nitrogen N, which become two of the most abundant species beginning at some distance behind strong shock waves in air, the electron impact ionization cross-sections are not very well known. However, judging from the fact that the cross-sections vs electron energy curves for all the observed molecules are similar except for a displacement in the threshold energy, and that they are also very similar to those observed for noble gas atoms,* it is reasonable to assume that the electron impact ionization cross-sections for O and N atoms are also quite similar to those for N_2, O_2, and NO, except for the difference in threshold energy. Therefore, in calculating the total electron impact ionization rate using the asymptotic formula (26), one may simply take $w_{iX}\bar{Q}'_{iX}$ (w_{iX}) $\cong \pi a_o^2$ for all the atoms as well as for the molecules.

The adoption of Eqs. (25) or (26) together with the cross-sections obtained from room temperature measurements may lead to an underestimate of the total electron impact ionization rate behind the shock due to the implicit neglect of multistep ionization via the upper electronic states.[2] However, such underestimate may have already been compensated for by our earlier assumption of identical electron and gas temperatures.

For ion-impact ionization [Reaction (16)], the cross-sections are generally much smaller than those for electron-impact ionization at energies below a few hundred electron volts.** Considering the fact that the heavier mass also tends to discourage the frequency of ion-neutral collisions, it becomes quite clear that the ion-impact processes will be insignificant in comparison with the electron-impact processes for producing ionization behind shock waves.

---

*H. S. W. Massey and E. H. S. Burhop, loc. cit., Section 6.4, p. 530.

**H. S. W. Massey and E. H. S. Burhop, loc. cit., Chapter VIII.

B. Photoionization

The rate of production of ion pairs per unit volume due to photoionization following a fluid element can likewise be expressed as

$$\left(\frac{dn_e}{dt}\right)_{(17)} = C \sum_X n_X \int_{w_{iX}/h}^{\infty} Q_{fX}(\nu)\, n(\nu)\, d\nu \qquad (27)$$

where C is the velocity of light; h is Planck's constant $Q_{fX}(\nu)$ is the photoionization cross-section for type X molecule at light frequency ν; and $n(\nu)\, d\nu$ is the local number density of photons in the frequency interval between ν and $\nu + d\nu$.

The far ultraviolet absorption spectra for N_2, O_2 and NO at room temperature have been studied by Weissler, Po Lee, and others.[33] The photoionization cross-section as deduced from these spectra[34] are reproduced here in Fig. 4 as functions of the photon energy $h\nu$. It is seen that the cross-section generally rises steeply from the threshold to a peak value of about 2×10^{-17} cm^2, and then decreases more gradually at higher photon energies. While the photoionization cross-sections for the atomic species N, O are not known, they are not likely to be very different from those of the molecular species, (after allowing for the differences in threshold energies) as one can judge from the observed cross-sections for other monatomic gases and metallic vapors.[34]

The peak value of about 2×10^{-17} cm^2 for the photoionization cross-sections implies that ionizing photons of energy substantially above the threshold may have a mean free path within the reaction zone behind the shock that is comparable to the thickness of the reaction zone itself. *

*The absorption mean free path for the ionizing photons at a local gas density ρ is then given by $\ell_\nu \cong 300 \ell_1 \rho_1/\rho$ where ℓ_1 and ρ_1 are respectively the viscosity mean free path and the gas density ahead of the shock. Thus, in the region behind the shock front where $\rho/\rho_1 \cong 10$, we have $\ell_\nu \cong 30 \ell_1$, which is comparable to the thickness of the reaction zone.

Thus, the local photon density $n(\nu)\, d\nu$ in the far ultraviolet can only be determined from a detailed consideration of the excitation, emission, and radiative transport problems within the reaction zone. These problems are generally quite complicated and the basic information required to treat these problems is at present only very coarsely known.[6, 35, 36] We shall, therefore, only attempt to make a rough estimate of the photoionization rate here.

From a study of the photoelectric measurements by Camm, et al,[35] Hammerling[37] has tentatively concluded that most of the far ultraviolet radiation from the reaction zone behind strong shock waves in air (up to $U_s = 7$ km/sec) may be attributed to the $b'\,{}^1\Sigma^+_u \longrightarrow X\,{}^1\Sigma^+_g$ transition of N_2. Neglecting absorption and re-emission, the total intensity of this radiation per unit area of the shock front may be expressed in the form

$$I \cong \frac{\bar{n}_{N_2} \exp\left(-E^*/kT^*\right)}{2\left(\tau_r + \tau_c\right)} \cdot E^* L \tag{28}$$

where $\bar{n}_{N2}$ is the averaged number density of N_2 molecules within the reaction zone; $E^* = 12.9$ e.v. is the energy difference between the two electronic states of N_2 (measured from their respective ground vibrational levels); L is the effective thickness of the reaction zone; τ_r and τ_c are respectively the radiative life time and collisional de-excitation time for the upper electronic state of N_2; and T^* is a temperature which characterizes the population of the electronic states of N_2 within the reaction zone when $\tau_c/\tau_r \longrightarrow 0$. By letting $Q_{fX}(\nu) = 2 \times 10^{-17}\ \text{cm}^2 = \pi a_o^2/4$ for all photon energies above the ionization threshold (i.e., $h\nu > w_{iX}$) and by equating I/E^* to the total ionizing photon flux density, one obtains, from Eqs. (27) and (28)

$$\left(\frac{dn_e}{dt}\right)_{(17)} \cong \frac{\pi a_o^2 \left(n_{O_2} + n_{NO}\right) \bar{n}_{N_2} L}{8\left(\tau_r + \tau_c\right)} \exp\left(-E^*/kT^*\right) \tag{29}$$

It may be noted that in arriving at the above expression, we have replaced $\sum_X n_X$ in Eq. (27) by $(n_{O_2} + n_{NO})$ since photons of 12.9 e.v. energy would only be sufficiently energetic to ionize O_2 and NO molecules, but not other chemical species behind the shock front. For numerical estimate of this photo-ionization rate, one may take, following the suggestion of Hammerling,[37] $\tau_r = 4 \times 10^{-9}$ sec;

$$\tau_c = (\bar{n}_{N_2} \; \bar{c}_{N_2} \; \bar{Q}_{N_2})^{-1}$$

where

$$\bar{c}_{N_2} = (8 \, k\bar{T} / \pi \, m_{N_2})^{1/2}$$

is the mean thermal speed of N_2 and $\bar{Q}_{N_2} \cong 5 \times 10^{-15}$ cm^2 is the gas kinetic (or viscosity) cross-section of N_2; and L to be twice the distance behind the shock front at which $T = T^*$. The effective temperature T^*, which is by far the most sensitive parameter in Eqs. (28) and (29), is somewhat uncertain. For fitting the limited experimental results by Camm, et al,[35] one may take $T^* \cong \frac{1}{2} (T_{x \to o} + T_{x \to \infty})$ where $T_{x \to o}$ is the gas temperature immediately behind the translational/rotational shock front, and $T_{x \to \infty}$ is the final equilibrium temperature far behind the shock.

C. Charge Exchange

The charge exchange reactions (18-a) and (18-b) involve a transfer of unit charge from one molecule (or atom) to another during a collision,[30, 38] and hence do not contribute to the net electron production rate during the early part of the ionization history. However, at later times when the electron-ion recombination rate becomes comparable to the ionization rate, such charge exchange reactions could influence the electron density profile through a continuous reshuffling of the relative populations among the different positive ions. This effect would especially be significant if there exists a large difference in recombination rates for the different kinds of positive ions (e.g., radiative recombination for atomic ions versus dissociative recombination for molecular ions).

For the oxygen-nitrogen system under consideration, the following specific reactions are of the straight forward type (18-a),

$$N_2^+ + N \rightleftharpoons N_2 + N^+ + 1.0 \text{ e.v.} \quad (30)$$

$$N_2^+ + O \rightleftharpoons N_2 + O^+ + 2.0 \text{ e.v.} \quad (31)$$

$$N_2^+ + O_2 \rightleftharpoons N_2 + O_2^+ + 3.5 \text{ e.v.} \quad (32)$$

$$N_2^+ + NO \rightleftharpoons N_2 + NO^+ + 6.3 \text{ e.v.} \quad (33)$$

$$N^+ + O \rightleftharpoons N + O^+ + 0.9 \text{ e.v.} \quad (34)$$

$$N^+ + O_2 \rightleftharpoons N + O_2^+ + 2.5 \text{ e.v.} \quad (35)$$

$$N^+ + NO \rightleftharpoons N + NO^+ + 5.3 \text{ e.v.} \quad (36)$$

$$O^+ + O_2 \rightleftharpoons O + O_2^+ + 1.6 \text{ e.v.} \quad (37)$$

$$O^+ + NO \rightleftharpoons O + NO^+ + 4.4 \text{ e.v.} \quad (38)$$

$$O_2^+ + NO \rightleftharpoons O_2 + NO^+ + 2.8 \text{ e.v.} \quad (39)$$

For these charge exchange reactions, quantitative information on the rate constant (or cross-section) is very meager, especially at the relatively low particle energy under consideration.[30] Existing data,[4, 38] however, seem to indicate that the cross-section for a typical exothermic charge transfer of this type at about 1 e.v. particle energy is of the order of a few times πa_o^2 (i.e., about 3×10^{-16} cm^2), which is not much smaller than the gas kinetic (momentum transfer) cross-section.

Charge exchange reactions of the type (18-b), which involve a simultaneous charge transfer and an explicit re-arrangement of atoms during a collision, include the following specific reactions,

$$N_2^+ + O \rightleftharpoons NO + N^+ - 2.2 \text{ e.v.} \quad (31\text{-a})$$

$$N_2^+ + O \rightleftharpoons NO^+ + N + 3.0 \text{ e.v.} \quad (31\text{-b})$$

$$N_2 + O^+ \rightleftharpoons NO + N^+ - 4.2 \text{ e.v.} \quad (31\text{-c})$$

$$N_2 + O^+ \rightleftharpoons NO^+ + N + 1.1 \text{ e.v.} \quad (31\text{-d})$$

$$N_2^+ + O_2 \rightleftharpoons NO + NO^+ + 4.5 \text{ e.v.} \quad (32\text{-a})$$

$$N_2 + O_2^+ \rightleftharpoons NO + NO^+ + 0.9 \text{ e.v.} \quad (32\text{-b})$$

$$O_2^+ + N \rightleftharpoons NO + O^+ - 0.2 \text{ e.v.} \quad (35\text{-a})$$

$$O_2^+ + N \rightleftharpoons NO^+ + O + 4.2 \text{ e.v.} \quad (35\text{-b})$$

$$O_2 + N^+ \rightleftharpoons NO + O^+ + 2.3 \text{ e.v.} \qquad (35\text{-c})$$

$$O_2 + N^+ \rightleftharpoons NO^+ + O + 6.7 \text{ e.v.} \qquad (35\text{-d})$$

While no quantitative information appears to be available in regard to the rate constants for these reactions, the similarity between these reactions and the neutral atom exchange reactions (4), (5), and (6) suggests that their corresponding exothermic rate constants may be of comparable magnitude. This would again place the exothermic cross-section for these reactions at about πa_o^2.

The third type of charge exchange reaction (18-c), which involves a simultaneous charge exchange with, and ionization of, the neutral particle, would be energetically possible only when the sum of the first and second ionization potentials of Y is comparable to the first ionization potential of X. This situation is not expected to occur in the dissociated air mixture. *

D. Electron Attachment

Atomic and molecular oxygen are known to have considerable electron affinity.[39-41] Thus, the attachment processes,

$$e + O_2 \rightleftharpoons O_2^- \qquad (40)$$

$$e + O_2 + X \rightleftharpoons O_2^- + X \qquad (40\text{-a})$$

$$e + O \rightleftharpoons O^- + h\nu \qquad (41)$$

$$e + O_2 \rightleftharpoons O + O^- \qquad (42)$$

$$e + NO \rightleftharpoons N + O^- \qquad (43)$$

which are typical examples of reactions (19-a), (19-b), and (19-c), often become the dominant rate-determining processes for the removal of free electrons in many ionospheric and gas-discharge situations.[29, 38, 42] However, in view of the fact that the binding energies for O_2^- and for O^-

*Note that even for alkali-earth elements, such as Ba and Ca, which may be present in small amounts as impurity in the gas sample, the sum of the first and second ionization potentials is still greater than 15 e.v.

are only about 0.5 and 1.5 e.v., respectively, the concentrations of O_2^- and O^- ions would always be negligibly small in comparison with the electron concentration whenever the gas temperature exceeds about 1,500°K. *

Even though the effect of these attachment processes on the ionization history is negligible, reactions (42) and (43) may contribute significantly to the dissociation rate of O_2 and NO at high electron temperature and density.

E. Ionizing Atomic and Molecular Collisions

From general considerations of inelastic collisions between two atomic systems under gas-kinetic conditions, one may conclude that ionizing collisions of the type represented by Eq. (20) would not be important as long as the mean kinetic energy per particle $\frac{3}{2}$ kT is small compared with the ionization potential w_{iX} of the atom (or molecule) being ionized. This conclusion can be arrived at either from a simple test of the near-adiabatic condition, **

$$\frac{a_o w_{iX}}{h\,(kT/m_X)^{1/2}} >> 1 \qquad (44)$$

or from the usual argument that energetic collisions between two particles in which the energy of relative motion exceeds the ionization potential are relatively rare.

While the above conclusion is certainly correct for noble gases in the range of gas temperature under consideration, [2] we must now consider the possibilities that the chemical energy in the colliding atomic systems may come into play so that the required amount of energy transfer from relative translational motion to electronic excitation may be considerably less than the ionization potential of the molecular complex formed by the collision.

---

*Even though collisional detachment by neutral atoms and molecules (see Ref. 41) may not be sufficiently rapid to keep the negative ions in quasi-equilibrium with the free electrons and the neutral particles, there is no reason why collisional detachment by electrons should not be sufficiently rapid to maintain such a quasi-equilibrium condition behind the shock front.

**See for example, Massey and Burhop, loc. cit., Chapt. II.

This may lead to a violation of the near-adiabatic condition (44) for a considerable fraction of all the molecular encounters even at gas temperatures of the order of 10^4 °K. Thus, in the presence of crossing,[43] or near-crossing, of the potential energy curves for the colliding atomic system (or potential energy surfaces in the case of collision between molecules), ionizing reactions of the types represented by (21) through (23-b) could be extremely rapid.

For the oxygen-nitrogen system under consideration, we may now make a representative (but not exhaustive) list of specific reactions which belong in this category according to an ascending order of their respective energy of reaction ΔE^o:

$$N + O + 2.8 \text{ e.v.} \rightleftharpoons NO^+ + e \quad (45)$$

$$N + N + 5.8 \text{ e.v.} \rightleftharpoons N_2^+ + e \quad (46)$$

$$N + O_2 + 6.5 \text{ e.v.} \rightleftharpoons NO_2^+ + e \quad (47)$$

$$O + O + 6.9 \text{ e.v.} \rightleftharpoons O_2^+ + e \quad (48)$$

$$O + NO + 7.9 \text{ e.v.} \rightleftharpoons NO_2^+ + e \quad (49)$$

$$N + NO + 7.9 \text{ e.v.} \rightleftharpoons N_2O^+ + e \quad (50)$$

$$X + NO + 9.3 \text{ e.v.} \rightleftharpoons X + NO^+ + e \quad (51)$$

$$O + N_2 + 11.2 \text{ e.v.} \rightleftharpoons N_2O^+ + e \quad (52)$$

$$N_2 + O_2 + 11.2 \text{ e.v.} \rightleftharpoons NO + NO^+ + e \quad (53)$$

$$O + O_2 + 11.7 \text{ e.v.} \rightleftharpoons O_3^+ + e \quad (54)$$

$$X + O_2 + 12.1 \text{ e.v.} \rightleftharpoons X + O_2^+ + e \quad (55)$$

$$X + O + 13.6 \text{ e.v.} \rightleftharpoons X + O^+ + e \quad (56)$$

$$X + N + 14.6 \text{ e.v.} \rightleftharpoons X + N^+ + e \quad (57)$$

$$X + N_2 + 15.6 \text{ e.v.} \rightleftharpoons X + N_2^+ + e \quad (58)$$

From an earlier study of the ionization rate behind shock waves in diluted O_2 - N_2 mixtures, Lin[44] has made a crude determination of the forward rate constant for reaction (45). The velocity-averaged cross-section associated with this process as deduced from these earlier experiments is reproduced here in Fig. 5. It may be mentioned that a correction factor of about 5 has been applied to the lower bound estimate presented in Ref. 44 to account for the effect of finite dissociation rate,* so that these results now represent more closely the true cross-section for this process within the temperature range covered by the experiments. To extrapolate these results to other temperatures, we shall proceed in the following manner:

According to Bates and Massey,[45] the cross-section associated with each energetically allowed ionizing collision (i.e., impact energy E greater than the activation energy E_x) due to potential energy curve crossing is expressible in the form

$$Q_{E > E_x} = g\pi (R_x a_o)^2 \left[1 - \exp\left(- 3.8 \times 10^{-15} \frac{\mu^{1/2} R_x}{E^{1/2} \tau_{A.I.}}\right)\right] \qquad (59)$$

where g is the ratio between the statistical weight associated with the initial potential energy curve which leads to the crossing point and the sum of the statistical weights associated with all possible initial potential energy curves of the colliding atomic system; $R_x a_o$ is the distance between the two centers of mass of the colliding system where the crossing occurs; $\mu = \mu_A \mu_B / (\mu_A + \mu_B)$ is the reduced molecular weight of the colliding system; E is the impact energy (measured in electron-volts); and $\tau_{A.I.}$ is the auto-ionization life time measured in seconds) of the molecular complex formed after the potential energy curve crossing, which is, of course, the main unknown in the problem. According to the works of Bransden and Dalgarno,[46] Wu,[47] and others, the

*The lower bound estimate presented in Ref. 44 was based on the experimentally observed ionization rate behind the shock but assuming that the O_2 - N_2 mixture was everywhere in dissociation equilibrium. More recent finite rate calculations indicated that the dissociation equilibrium assumption has overestimated the local atom concentrations by a considerable factor.

auto-ionization time for some typical doubly-excited states of helium appears to lie in the range $10^{-15} < \tau_{A.I.} < 10^{-11}$ sec., but no quantitative information appears to exist for more complex atomic systems.

The potential energy curves for the lower electronic states of the N + O and the $N + O^+$ systems are illustrated in Fig. 6. It is seen that there exist several possibilities for crossing of the N + O curves near the potential energy minimum of the $^1\Sigma^+$ state of NO^+. One may therefore interpret the experimental result shown in Fig. 5 as due to such curve-crossing. Thus, for the system under consideration, we have, $\mu = 7.5$; $R_x\, a_o \cong 10^{-8}$ cm; and $E_x \cong 3$ e.v. If $\tau_{A.I.}$ were much shorter than 10^{-14} sec, Eq. (59) becomes approximately,*

$$Q_{E > E_x} \cong g\pi (R_x\, a_o)^2 \cong 3 \times 10^{-17} \quad cm^2 \tag{59-a}$$

Behind the translational/rotational shock front, the velocity distribution of the atoms and molecules will be approximately Maxwellian at the local translational temperature T. The velocity-averaged ionization cross-section would then be,[48]

$$\bar{Q} \cong 3 \times 10^{-17} (E_x/kT) \exp(-E_x/kT) \quad cm^2 \tag{60-a}$$

On the other hand, if $\tau_{A.I.}$ were much longer than 10^{-14} sec., Eq. (59) becomes approximately

$$Q_{E > E_x} \cong 6 \times 10^{-31} (E^{1/2}\, \tau_{A.I.})^{-1} \quad cm^2 \tag{59-b}$$

Assuming $\tau_{A.I.}$ to be independent of impact energy, the corresponding velocity-averaged cross-section becomes,

$$\bar{Q} \cong 3 \times 10^{-31} (E_x^{1/2}\, \tau_{A.I.})^{-1} \left(\frac{E_x}{kT}\right) \exp\left(-\frac{E_x}{kT}\right) \quad cm^2 \tag{60-b}$$

---

*For the $N(^4S) + O(^3P)$ system, g would be either 1/18 or 2/9, depending on whether the $^2\Sigma^+$ or the $^4\Pi$ state is involved in the crossing. Therefore, a reasonable number to be assigned to g would be 0.1 when the state involved is not known.

If one tries to fit the center of the experimental points shown in Fig. 5 to Eq. (60-a), which has only one adjustable parameter (assuming that only one crossing point was involved in the experimental situation), one obtains $E_x = 4.8$ e.v., and

$$\bar{Q} = 1.7 \times 10^{-12} T^{-1} \exp(-55,700/T) \quad cm^2 \qquad (61\text{-a})$$

which gives the steepest possible temperature dependence (dotted curve in Fig. 5). On the other hand, if we let $E_x = 2.8$ e.v., which is the lowest possible activation energy for reaction (45), fitting the center of the same set of experimental points to Eq. (60-b) yields $\tau_{A.I.} = 6 \times 10^{-13}$ sec, and

$$\bar{Q} = 10^{-14} T^{-1} \exp(-32,500/T) \quad cm^2 \qquad (61\text{-b})$$

which gives the weakest possible temperature dependence (solid curve in Fig. 5). Since the limited temperature range and the considerable scatter of the experimental points as shown in Fig. 5 do not allow a better determination of the temperature dependence within the above two possible extremes, we shall draw on some other experimental evidence for such a determination.

The forward rate constants (i.e., the mean cross-section multiplied by the mean thermal speed based on the reduced mass of the two colliding atoms) corresponding to (61-a) and (61-b) are, respectively,

$$\kappa_{45\,(a)} \cong 9 \times 10^{-9} T^{-1/2} \exp(-55,700/T) \quad cm^3/sec \qquad (62\text{-a})$$

$$\kappa_{45\,(b)} \cong 5 \times 10^{-11} T^{-1/2} \exp(-32,500/T) \quad cm^3/sec \qquad (62\text{-b})$$

Within the temperature range $300 \leq T \leq 30,000^{\circ}K$, the equilibrium constant for reaction (45) can be approximated by the polynomial (to an accuracy of about $\pm$ 10%, assuming no error in the energy of reaction),

$$K_{45} \cong (1.4 \times 10^{-8} T + 1.2 \times 10^{-12} T^2 + 1.4 \times 10^{-16} T^3) \exp(-32,500/T) \qquad (63)$$

Dividing (62-a) and (62-b) by (63), one obtains the corresponding backward rate constants for reaction (45), which, at low temperatures (i.e., $T << 10^4\ ^oK$), become approximately,

$$\kappa_{R45(a)} \cong 6 \times 10^{-1}\ T^{-3/2} \exp(-23,200/T) \quad cm^3/sec \qquad (64\text{-a})$$

$$\kappa_{R45(b)} \cong 3 \times 10^{-3}\ T^{-3/2} \quad cm^3/sec \qquad (64\text{-b})$$

Note that the steep temperature dependence (64-a) would rule out any experimental observation of dissociative recombination for NO^+ at or near room temperature, since the numerical value of $\kappa_{R45(a)}$ would then be of the order of 10^{-38} cm^3/sec. On the other hand, the weak temperature dependence (64-b) gives $\kappa_{R45(b)} \cong 6 \times 10^{-7}$ cm^3/sec at 300^oK, which is quite compatible with the dissociative recombination coefficient of about 2×10^{-6} cm^3/sec deduced by Doering and Mahan[49] from photolysis of NO. At a temperature of 2000^oK, the same equation gives $\kappa_{R45(b)} \cong 3 \times 10^{-8}$ cm^3/sec, which is also compatible with Sugden's observation* that the dissociative recombination coefficient for NO^+ at flame temperatures appeared to be of the order of 10^{-7} cm^3/sec. Therefore, these low temperature experiments seem to support the weak temperature dependence (62-b) and (64-b) for the rate constants of reaction (45).

A question may be raised here in regard to the validity of comparing the forward and backward rates for reaction (45) in the above manner, as the electronic states of the atoms and the detailed paths associated with the observed rates are not known. Actually, in order for the above comparison to be valid, a sufficient condition would be that the rate governing step was in the potential energy curve crossing, and that both the forward and the backward processes passed through the same crossing point. It may further be noticed that this also happened to be a necessary condition

*T. M. Sugden, discussion following Doering and Mahan's paper, loc. cit.

in order to explain Sugden's flame temperature result.*

For reactions (46) and (48), while no quantitative measurement of the forward rate constants has yet been made, the recombination rates for electrons and N_2^+, O_2^+ ions have been a subject of study for some time in gas discharge.[30] The recent work of Kasner, Rogers, and Biondi,[50] which confirmed the existence of dissociative recombination in the after glow decay of a microwave discharge through the use of a mass spectrometer, indicated that the recombination coefficients for N_2^+ ions and electrons and for O_2^+ ions and electrons are $(5.9 \pm 1.0) \times 10^{-7}$ cm^3/sec and $(3.8 \pm 1.0) \times 10^{-7}$ cm^3/sec, respectively. Since the electron temperature relaxation time was generally much shorter than the time over which the dissociative recombination process was observed under the experimental conditions described by Kasner, et al,[50] the electron temperature could not have been much higher than the gas temperature in the decaying after glow. Thus, the magnitude of the observed rate constants suggested that the dissociative recombination of electrons and N_2^+, O_2^+ ions also did not require any noticeable amount of activation energy. Again, if one attributes these dissociative recombination processes to the crossing of potential energy curves, the crossing points must also have occurred near the corresponding potential energy minima of the $e + N_2^+$ and the $e + O_2^+$ system, and the auto-ionization times associated with the corresponding N_2 and O_2 complexes must also be of the order of 10^{-12} second. Such interpretation of the observed low temperature dissociative recombination

---

*Interpretation of Sugden's result presents no difficulty if the dissociative recombination process results in ground state N and O atoms. On the other hand, if the process were $e + NO^+(^1\Sigma^+) \rightleftharpoons N(^2D) + O(^3P) + 0.4$ e.v. or, $e + NO^+(^1\Sigma^+) \rightleftharpoons N(^4S) + O(^1D) + 0.8$ e.v. the recombination process could not proceed very far at flame temperatures on account of the very low energy of reaction (which favors the ionized state) unless de-excitation of the N (^2D) or O (^1D) states were sufficiently rapid. This implies that unless the rate governing step were in the potential energy curve crossing and not in the collisional de-excitation of metastable atoms, the recombination rate at flame temperatures should be very different from that at room temperature.

coefficients also leads to the following temperature-dependent backward rate constants for reactions (46) and (48).

$$\kappa_{R46} \cong 3 \times 10^{-3}\, T^{-3/2} \quad \text{cm}^3/\text{sec} \tag{65}$$

$$\kappa_{R48} \cong 2 \times 10^{-3}\, T^{-3/2} \quad \text{cm}^3/\text{sec} \tag{66}$$

It may be noted that the $T^{-3/2}$ temperature dependence for the backward rate constants is the same as that suggested by Sayers,[4] but that the numerical coefficients for κ_{R46} and κ_{R48} as shown are smaller than his suggested values by factors of about 5 and 1.5, respectively. To obtain the forward rate constants, one may multiply (65) and (66) by the corresponding equilibrium constants for reactions (46) and (48), which, in the temperature range $300 \leq T \leq 30,000^{\circ}\text{K}$, may be approximated by the polynomials (again to an accuracy of about $\pm$ 10%, assuming no error in the energy of reaction),

$$K_{46} \cong (3 \times 10^{-8}\, T + 4 \times 10^{-12}\, T^2 + 10^{-15}\, T^3 - 3 \times 10^{-20}\, T^4) \exp(-67,300/T) \tag{67}$$

$$K_{48} \cong (1.6 \times 10^{-8}\, T + 1.2 \times 10^{-12}\, T^2 + 3.5 \times 10^{-16}\, T^3) \exp(-80,100/T) \tag{68}$$

These yield,

$$\kappa_{46} = K_{46}\, \kappa_{R46} \cong 9 \times 10^{-11}\, T^{-1/2} (1 + 1.3 \times 10^{-4}\, T + 3.3 \times 10^{-8}\, T^2 - 10^{-12} T^3) \exp(-67,300/T) \text{ cm}^3/\text{sec} \tag{69}$$

$$\kappa_{48} = K_{48}\, \kappa_{R48} \cong 3.2 \times 10^{-11}\, T^{-1/2} (1 + 7.5 \times 10^{-5}\, T + 2.2 \times 10^{-8}\, T^2) \exp(-80,100/T) \quad \text{cm}^3/\text{sec} \tag{70}$$

For the molecule-molecule collision processes (53), (55) and (58), one may deduce the corresponding forward rate constants from the recent molecular beam results of Utterback and Miller[51] and Utterback.[52,53] The monochromatic (i.e., single-energy) ionization cross-sections for N_2 - N_2, N_2 - O_2, and O_2 - O_2 collisions as reported in Refs. 51 and 53 are reproduced here in Fig. 7. By extrapolating the linear portion of these curves

toward $(E - E_i) \longrightarrow 0$, and integrating according to the Maxwellian molecular velocity distribution,[48] one obtains the following expressions for the forward rate constants for reactions (53), (55) and (58),

$$\kappa_{53} = \kappa_{55}^{N_2} = 4.5 \times 10^{-25} T^{5/2} (1 + 3 \times 10^{-5} T) \exp(-141,000/T) \text{ cm}^3/\text{sec} \quad (71)$$

$$\kappa_{55}^{O_2} = 1.1 \times 10^{-33} T^{9/2} (1 + 4 \times 10^{-5} T) \exp(-141,000/T) \text{ cm}^3/\text{sec} \quad (72)$$

$$\kappa_{58}^{N_2} = 2.8 \times 10^{-28} T^{7/2} (1 + 3 \times 10^{-5} T) \exp(-181,000/T) \text{ cm}^3/\text{sec} \quad (73)$$

It is interesting to note that at temperatures below 30,000°K, the pre-exponential factors for $\kappa_{55}^{O_2}$, $\kappa_{55}^{N_2}$, and $\kappa_{58}^{N_2}$ shown above are somewhat smaller than those for $\kappa_{45(b)}$, κ_{46} and κ_{48} given in Eqs. (62-b), (69) and (70), but at T = 30,000°K, they become comparable. This suggests that the ionization processes for the $O_2 - O_2$, $N_2 - O_2$ and $N_2 - N_2$ collisions observed by Utterback and Miller in the molecular beam experiments may also be interpreted as due to crossing of the potential energy hypersurfaces for the colliding molecular systems.* The steep energy dependence of the observed ionization cross-section (see Fig. 7), however, indicates that the corresponding auto-ionization time $\tau_{A.I.}$ associated with these molecular collisions is not independent of impact energy.

For reactions (47), (49), (50), (51), (52), (54), (56), (57), and for reactions (55), (58) when the colliding particle X is other than O_2, N_2, there seems to be no direct experimental information available in the literature. However, in view of the general trend which has just been established between the rate constants for those reactions where experimental information is available, it is not unreasonable to express the forward rate constants for all these reactions in the simple Arrhenius form,

$$\kappa_j = A_j (T) \exp(-\Delta E_j^o / kT) \quad (74)$$

*H. S. W. Massey and E. H. S. Burhop, loc. cit., p. 450.

and to make A_j (T) comparable to either the pre-exponential factors for $\kappa_{45(b)}$, κ_{46}, κ_{48} or those for κ_{53}, $\kappa_{55}{}^{O_2}$ and $\kappa_{58}{}^{N_2}$.

It may be pointed out that in a recent treatment of the ionization relaxation problem in hypersonic air flows, Hall, Eschenroeder, and Marrone,[17] and Eschenroeder[54] have made estimates of the backward rate constants for reactions (55) through (58) according to Thomson's three-body recombination theory.[55] They have subsequently arrived at rate constants that are in effect many orders of magnitude greater than what we have just proposed above for these unknown reactions in the temperature range of interest (i.e., $T \leq 30,000^{\circ}K$). In view of the fact that such large rate constants are not consistent with the crossing point model (assuming any reasonable value for the auto-ionization time $\tau_{A.I.}$), and the fact that the classical Thomson theory is probably not applicable to electron-ion recombination,* these high estimates may be tentatively disregarded.

IV. RESULTANT IONIZATION HISTORY BEHIND THE SHOCK

By numerical integration of the various ionization rate equations according to the local temperature and neutral particle concentrations already determined (see Section II), one obtains the instantaneous electron production rate as well as the electron and positive ion densities as functions of distance behind the shock. The specific ionization rate due to the various groups of processes is plotted in Fig. 8 for three typical shock velocities. The initial air density chosen for these numerical examples is $p_1 = 0.02$ mm Hg at room temperature, but to show the density dependence, the specific ionization rate at $p_1 = 2$ mm Hg is also plotted in Fig. 8(b). The specific ionization rate is defined here as the absolute value of the time rate of change of the normalized electron density (following the mass motion of the fluid) multiplied by the time it takes the shock to traverse one upstream mean free path, ℓ_1/U_s (which is also roughly the mean binary collision time behind the shock). The curve labeled "atom-atom" refers to the sum of the contributions from reactions (45), (46) and (48), which are calculated according to equations analogous

*H. S. W. Massey and E. H. S. Burhop, loc. cit., p. 623.

to Eq. (7-a), using backward rate constants given by (64-b), (65), (66) and corresponding forward rate constants given by

$$\kappa_j = K_j \kappa_{Rj} \tag{75}$$

where K_j is the equilibrium constant for the particular reaction (j). It may be noted that for reaction (45), the forward rate constant so specified becomes somewhat greater than that corresponding to Eq. (62-b) at high temperatures (by a factor of about 2.4 at 10,000°K; and about 5.6 at 20,000°K). This method of extrapolating κ_{45} to higher temperatures is probably more realistic than a direct application of Eq. (62-b) in view of the noted steep temperature dependence for κ_{53}, $\kappa_{55}^{O_2}$, and $\kappa_{58}^{N_2}$. The curve labeled "Molecule-Molecule and Atom-Molecule" refers to the sum of the contributions from reaction (47) and reactions (49) through (58). The contributions from reactions (53), (55) and (58) are calculated according to the forward rate constants given by Eqs. (71), (72) and (73); while the contributions from all other reactions in this group are calculated according to Eq. (74), using a pre-exponential factor given by the geometrical mean of those for κ_{45}, κ_{46}, κ_{48}, κ_{53}, $\kappa_{55}^{O_2}$, and $\kappa_{58}^{N_2}$.

The curve labeled "Electron Impact" is calculated according to Eq. (26), taking $w_{iX}\Omega'_{iX}(w_{iX}) = \pi a_o^2$ for all species. The curve labeled "Photoionization" is calculated according to Eq. (29), with a simple correction factor $\exp\left[-\beta\ (x-L)\right]$ to allow for attenuation of the far u.v. intensity at large distances behind the shock, using an absorption coefficient given by $\beta \cong 10^{-17}\sum_X n_X\ \text{cm}^{-1}$.

In these specific rate calculations, the charge exchange reactions (30) through (39) and (31-a) through (35-d) are allowed to proceed simultaneously with the electron production processes. The rate constants for these 20 charge exchange reactions are based on exothermic charge transfer cross-section of $3\pi a_o^2$, as explained in Section III-C.

According to these numerical results, the most important group of ionization processes appears to be the atom-atom reactions. This is to be followed in an approximately decreasing order of importance by photoionization, electron impact, atom-molecule, and molecule-molecule collisions, depending on the shock velocity. The predominance of the atom-atom

processes is most pronounced at low shock velocities on account of their advantage in activation energy. The electron-impact processes, on the other hand, make negligible contributions at shock velocities below 5 km/sec., but may become the predominant processes at shock velocities greater than 10 km/sec.

Comparing the results plotted in Fig. 8(b) for the two values of p_1 which differ by a factor of 100, it is seen that these specific ionization rates are relatively density-independent. This is due to the predominance of the two-body processes in the range of air density under consideration.

Among the atom-atom ionization processes, the N-O reaction (45) appears to be the major contributor within the range of shock velocity under consideration. This is illustrated in Fig. 9, where the partial contributions from the various atom-atom, atom-molecule, and molecule-molecule processes are plotted for the case $U_s = 6.9$ km/sec and $p_1 = 0.02$ mm Hg. The predominance of reaction (45) over the other reactions is more pronounced at lower shock velocities, but at $U_s \cong 9$ km/sec the contribution from the N-N reaction (46) becomes comparable to that from the N-O reaction. It may be noted that the curves (45-R), (46-R) and (48-R), as well as the curves labeled "atom-atom, $(d[e]/dt < 0)$" in Figs. 8(a), (b) and (c), refer to the rate of disappearance of free electrons due to the excess of the backward rate (i.e., dissociative recombination) over the corresponding forward rate.

The normalized electron and ion densities are plotted in Figs. 10(a), (b), and (c) as functions of the normalized distance for the same shock conditions as those illustrated in Figs. 8(a), (b), and (c). It is seen that the electron density generally builds up monotonically until the atom-atom reactions run into reverse. Beyond this point, the electron density is continuously reduced by dissociative recombination as the atom-atom reactions try to follow the decreasing translational temperature toward the final equilibrium level.

Among the positive ions, NO^+ is expected to be the most abundant species up to fairly high shock velocity. However, at about 9 km/sec velocity, the atomic ions N^+ and O^+ may become more abundant than NO^+ at some distance behind the shock. This is to be expected at high temperatures in the presence of quasi-statistical equilibrium between the various positive ions

brought about by the rapid charge exchange reactions. It may be mentioned that in the numerical calculations, radiative recombination between the atomic ions and electrons has been neglected so that the production and destruction of these ions were completely governed by the charge exchange reactions.

The effect of changing the charge exchange reaction rate on the resultant electron and ion density distributions behind the shock is illustrated in Fig. 11 for the case $U_s = 6.9$ km/sec, and $p_1 = 0.02$ mm Hg. In this figure, the resultant distributions of $[e]$, $[N^+]$, $[O^+]$, and $[O_2^+]$ obtained by increasing and decreasing the adopted exothermic charge exchange cross-section $Q_{ch.\,ex} = 3\pi a_o^2$ by a factor of 100 are plotted for comparison with those obtained from the adopted cross-section. The distributions of $[NO^+]$, $[N_2^+]$ showed much smaller changes than those for the other positive ions and hence are not plotted. It is seen that the maximum effect on $[e]$, which occurs in the neighborhood of the peak electron density, is only of the order of 10 percent. For the positive ions; the small effect of increasing $Q_{ch.\,ex}$ by a factor of 100 indicates that the adopted cross-section was already sufficiently large to keep the various ions in quasi-statistical equilibrium. In fact, the relatively mild changes in $[N^+]$, $[O^+]$, and $[O_2^+]$ obtained by decreasing $Q_{ch.\,ex}$ by a factor of 100 shows that it would indeed be difficult to keep the various ions away from the state of quasi-statistical equilibrium behind the shock.

Before leaving this section, we shall now examine briefly the effects of upstream photoionization and electron diffusion on the resultant ionization profile behind the shock. From the experimental observation of Camm, Kivel, Taylor, and Teare,[35] it is quite clear that sufficiently energetic photons could escape from the translational/rotational shock front to photoionize molecular oxygen upstream. The production of free electrons ahead of a plane shock wave by this "precursor radiation" has been treated in some detail by Hammerling in Ref. 37. There is also evidence of such photoionization effect being observed during satellite re-entry.[56] In the present discussion, however, we need only to estimate the cumulative effect of such upstream photoionization on the resultant ionization history behind the shock.

The electron density distribution behind the shock with and without considering upstream photoionization is shown in Fig. 12 for the case $U_s = 6.9$ km/sec and $p_1 = 0.02$ mm Hg. The solid curve, with no upstream photoionization and identical to that shown in Fig. 10(b), was obtained by integrating the specific ionization rates behind the shock, assuming $[e] = 0$ at $x = 0$. The dotted curve, on the other hand, was obtained by integrating the same set of rate equations, but letting $[e] = 10^{-4}$ at $x = 0$. This initial value of $[e]$ was obtained by a balance between the outgoing ionizing photon flux ($h\nu \geq 12.1$ e.v.) observed by Camm, et al[35] [see Eq. (28)] and the flux of ion pairs convected back into the translational/rotational shock front per unit area due to the mass motion of the fluid. It is seen that even though the neglect of upstream photoionization would lead to serious error in the very early part of the ionization history, by the time $[e]$ reaches about 10 percent the peak value behind the shock, the error involved becomes smaller than a factor of two in this case. It may be pointed out, however, that such error would be somewhat more severe at higher shock velocities on account of the increasing importance of the electron impact ionization process with shock velocity [compare Figs. 8(b) and (c)].

In regard to the effect of electron diffusion, one may note that even at $p_1 = 0.02$ mm Hg, the Debye shielding distance[57]

$$h_D = \left(kT/4\pi n_e e^2 \right)^{1/2} \tag{76}$$

corresponding to the electron density profiles illustrated in Fig. 10(a) through 12 is always less than 5×10^{-2} cm. This is sufficient to insure ambipolar diffusion[29, 38] and charge neutrality down to a distance scale smaller than $0.2\,\ell_1$. Since ambipolar diffusion is not much more rapid than momentum (or viscosity) diffusion, it can again be neglected outside the translational/rotational relaxation zone.

V. COMPARISON WITH EXPERIMENT

The theoretical results obtained above may now be used for comparison with the experimental observations of Lin, Fyfe and Neal reported in the complementary paper (Ref. 1). Since no direct experimental determination of the positive ion distribution has yet been made, we shall restrict our attention to the electron density distribution.

The theoretical electron density profile in physical scales for the case U_s = 6.9 km/sec, p_1 = 0.02 mm Hg is plotted in Fig. 13 for comparison with the electron density profile obtained from four separate experiments taken at $U_s = 6.9 \pm 0.05$ km/sec, at the same initial air pressure. Curve (1) is identical to the normalized curve [e] shown in Fig. 10(b). Curves (2) and (3) are reference curves obtained by changing the absolute rate constant for the predominant ionizing reaction (45) by a factor of three in either directions (i.e., taking $\kappa_{R45} = 9 \times 10^{-3} T^{-3/2}$ and $\kappa_{R45} = 1 \times 10^{-3} T^{-3/2}$, respectively), while holding all other rate constants the same as those specified in the preceding section. The effect of upstream photoionization is hardly noticeable in this linear plot since the initial electron density amounts to only about 7×10^{10} electrons/cm^3 just ahead of, and 4×10^{11} electrons/cm^3 just behind the translational/rotational shock front.

It is seen that the front part of the experimentally observed profile appears to fall between curve (1) and curve (2) but the rear part of the observed profile seems to fall systematically above the theoretical curves. Even though the apparent discrepancy of the order of 20 percent is still within the probable inaccuracy of the experiment in absolute electron density determination,[1] the distinct difference in slope between the theoretical and experimental profiles may be significant. However, in view of the fact that no reasonable adjustment of either the ionization or the chemical rate constants could reduce the theoretical rate of decrease of electron density behind the peak to the experimentally observed rate, it is believed that the slower observed rate of decrease of n_e at large distances behind the shock front was due to the slight deceleration of the shock wave in the experimental situation.[6] In a decelerating shock wave, the fluid elements further away from the shock front are those that have been heated by a stronger shock wave, so that the resultant perturbation is in the direction of reducing the rate of decrease of translational temperature behind the shock.

The theoretical peak electron density and the maximum electron density gradient behind the shock at initial air pressure p_1 = 0.02 mm Hg are plotted in Figs. 14 and 15, as functions of the shock velocity (or the shock Mach number $M_s = U_s/a_1$, where a_1 is the speed of sound for air at room temperature). This may be compared with the corresponding measured

quantities presented in Figs. 8 and 10 of Ref. 1. The theoretical curves (1), (2) and (3) are again based on the electron density profiles calculated according to $\kappa_{R45} = 3 \times 10^{-3}\ T^{-3/2}$; $9 \times 10^{-3}\ T^{-3/2}$; and $1 \times 10^{-3}\ T^{-3/2}$, respectively. The electron density corresponding to the final equilibrium value far behind the shock is also plotted for comparison. It is seen that the amount of "ionization overshoot" observed in the experiment[1,6] was perfectly reasonable according to the present theoretical model, even though the relative insensitivity of the peak electron density to the ionization rate makes this quantity a poor measure of the rate constant. The maximum electron density gradient shown in Fig. 15, on the other hand, is sensitive to the ionization rate and shows a clear preference for curves (1) and (2) over curve (3). It is also interesting to note that according to these calculations, the "ionization overshoot" phenomenon is expected to disappear at shock velocities below 4 km/sec and above 9 km/sec.

The theoretical "ionization rise distance" and "ionization incubation distance" are plotted in Figs. 16 and 17 for comparison with the corresponding experimental results presented in Figs. 11 and 12 of Ref. 1. These quantities are defined here as the peak electron density divided by the maximum electron density gradient; and the distance for the local electron density to reach one-half the peak value behind the shock, respectively. The curves (1), (2) and (3) have the same meaning as before. It may be noted that the experimental points presented include measurements both from the microwave reflection probe (hollow points) and from the magnetic induction probe (solid points). The microwave probe measured the electron density directly, but the magnetic probe measured only the d. c. electrical conductivity, which is related to the electron density by

$$\sigma_{d.c.} = n_e e^2/m_e \nu_e \qquad (77)$$

However, within the range of shock strength covered by the experiments, (i. e., $U_s \leq 7$ km/sec), the electron collision frequency ν_e calculated according to the theoretical temperature, density and chemical composition profiles (Section II) and the published values for the electron momentum transfer cross-sections for the various species[58] does not vary by more than a factor of 2 with distance behind the shock front, while the electron density

changes by orders of magnitude. Therefore, the measurements obtained by both methods may be compared directly with the theoretical curves. It is seen that the experimental points are in reasonably good agreement with the geometrical mean of curves (1) and (2).

The initial pressure dependence of the peak electron density and of the maximum electron density gradient behind the shock reported in Ref. 1 may be interpreted as a direct consequence of the predominance of binary collisions in the forward rate processes within the range of gas density under consideration. This is perfectly consistent with the theoretical results [see Figs. 1, 2, 8(b) and 10(b)].

VI. DISCUSSIONS

From the foregoing results, it is seen that all the experimental observations reported in Ref. 1 can be satisfactorily interpreted according to the present theoretical model. Even though many of the ionization rate constants are still uncertain, comparison of the specific rates based on tentative rate constants [see Figs. 8(a), (b), (c) and 11] showed that only a few of them are pertinent. Therefore, the number of rate constants that can be adjusted to fit the experimental results is actually quite limited. In fact, the apparent predominance of the atom-atom reactions throughout the range of shock velocity under consideration showed that only through an adjustment of the rate constant for reaction (45), and to a lesser extent, the rate constants for reactions (46) and (48), can one effectively alter the ionization profile behind the shock.

The reasonably close (i. e. , within a factor of 2) agreement between the experimental points and the theoretical curve (1) shown in Figs. 13 through 17 suggests that the assignment of κ_{R45}, κ_{R46}, and κ_{R48} according to Eqs. (64-b), (65) and (66) is already quite satisfactory. Even though an upward revision of κ_{R45} by a factor of 2 would bring the theoretical curve to near perfect agreement with the experimental points, such a fine adjustment may not be justified at this time in view of the existence of other uncertainties in the theoretical model which could be of comparable magnitude. These include, especially, uncertainties in the chemical composition profile caused by uncertainties in the high temperature dissociation rate constants,[6,15] and in the model of coupling between vibrational relaxation and dissociation.

The theoretical results presented here may be extended over a much wider range of initial air density without difficulty. The upper density limit is

reached when the rates of dissociation and ionization due to three-body collisions (comparing only the forward rates) become comparable to those due to binary collisions. This is not expected to occur at densities much below liquid air density. For extension to lower densities, while there seems to be no theoretical limit, a practical limit should be set by the realizability of air samples without excessive contamination from the vapor pressure of the container, or from the environment, if the theoretical results were to be compared with experimental observations.

The theoretical calculation can readily be extended to other initial O_2/N_2 mixture ratios, and also to predissociated oxygen-nitrogen mixtures for upper atmosphere application. With minor modification, the effects of adding small amounts of argon, CO_2, H_2O and other gases to the mixture may also be estimated, using rate constants of the form given by Eq. (74). Contributions to the electron impact ionization rates by these extra gases can readily be included in Eq. (26).

Extension of the present theoretical model to a wider range of shock strength, on the other hand, represents a more complicated problem. As already mentioned earlier, extension of the shock velocity above 10 km/sec not only requires better knowledge of the electron impact ionization rates (Section III-A), but also necessitates consideration of the two-way coupling between the dissociation processes and the ionization processes. Extension of the shock velocity below 4 km/sec is a lesser problem, but one must then consider the increasing role of impurities having low ionization potentials with decreasing gas temperature.

One remark may also be made concerning the applicability of the present one-dimensional results to three-dimensional problems. As is well known in fluid dynamics,[59] there is a one-to-one correspondence between the flow across an oblique shock wave and the flow across a normal shock wave. Therefore, the present results are directly applicable to plane oblique shock waves provided that only the normal component of the up-stream flow velocity is used to determine the shock strength, and that the distance scale refers to the normal distance from the shock surface. With slight modifications, the present model can also be used to follow the ionization history in the three-dimensional inviscid flow field of hypersonic objects[10,60] and in high-enthalpy nozzle flows.[61]

ACKNOWLEDGMENT

The authors wish to acknowledge the able assistance of Mr. Richard L. Johnson in writing the computer program and in obtaining the numerical results presented here. They also wish to thank Dr. Naple G. Utterback, University of Denver, for sending them a preprint of his recent paper (Ref. 53) before its appearance in the literature.

This work has been sponsored by the Electronics Research Directorate of the Air Force Research Division, Air Research and Development Command.

REFERENCES

1. Lin, S. C., Neal, R. A., and Fyfe, W. I., "Rate of Ionization behind Shock Waves in Air I. Experimental Results," Avco-Everett Research Laboratory Research Report 105, (1960); also, Phys. Fluids, December, 1962.

2. Petschek, H., and Byron, S., Annals of Physics, 1, 270 (1957).

3. Bond, J. W., Jr., Phys. Rev., 105, 1683 (1957).

4. Wray, K., Teare, J. D., Kivel, B., and Hammering, P., "Relaxation Processes and Reaction Rates behind Shock Fronts in Air and Component Gases," Avco-Everett Research Laboratory Research Report 83 (1959).

5. Hammerling, P., Teare, J. D. and Kivel, B., Proceedings of the Fourth International Conference on Ionization Phenomena in Gases (N. R. Nilsson, Ed.) North-Holland Publishing Company, Amsterdam (1960), p. IV D, 1092.

6. Lin, S. C., and Fyfe, W. I., Phys. Fluids, 4, 238 (1961).

7. Hammerling, P., Teare, J. D., and Kivel, B., Phys. Fluids, 2, 422 (1959).

8. Lin, S. C., and Teare, J. D., Bull. Am. Phys. Soc., Ser. II, 4, 195 (1959).

9. Duff, R. E. and Davidson, N., J. Chem. Phys. 31, 1018 (1959)

10. Lin, S. C., and Teare, J. D., "A Streamtube Approximation for Calculation of Reaction Rates in the Inviscid Flow Field of Hypersonic Objects," Proc. of the 6th Symposium on Ballistic Missile and Aerospace Technology (Morrow, Ely, Smith, Ed.), Academic Press, N. Y. (1961), Vol. IV, p. 35.

11. Freedman, E., and Daiber, J. W., J. Chem. Phys., 34, 1271 (1961).

12. Wray, K. L., and Teare, J. D., J. Chem. Phys., 36, 2582 (1962).

13. Kaufman, K., and Kelso, J., J. Chem. Phys. 23, 1702 (1955).

14. Davidson, N., "Selected Reactions Involving Nitrogen and Oxygen," Avco-Everett Research Laboratory Research Report 32 (1958).

15. Wray, K. L., "Chemical Kinetics of High Temperature Air," Avco-Everett Research Laboratory Research Report 104 (1961); also, Progress in Astronautics and Rocketry, Vol. 7 (F. Riddell, ed.), Academic Press, New York (1962), p. 181.

16. Vaglio-Laurin, R., and Bloom, M.H., "Chemical Effects in External Hypersonic Flows," Progress in Astronautics and Rocketry, Vol. 7, (F. Riddell, ed.), Academic Press, New York (1962), p. 205.

17. Hall, J.G., Eschenroeder, A.Q., and Marrone, P.V., "Inviscid Hypersonic Air-Flows with Coupled Non-equilibrium Processes," Inst. Aerospace Sci. Paper No. 62-67 (1962).

18. Blackman, V.H., J. Fluid Mech. 1, 61 (1956).

19. Camac, M., J. Chem. Phys. 34, 448 (1961).

20. Montroll, E.W., and Shuler, K.E., J. Chem. Phys. 26, 454 (1957).

21. Courant, R., and Friedrichs, K.O., "Supersonic Flow and Shock Waves," Interscience, New York (1948), p. 121-125.

22. Talbot, L., American Rocket Society Journal, 32, 1009 (1962).

23. Gilmore, F.R., "Equilibrium Composition and Thermodynamic Properties of Air to 24,000°K," Rand Corporation, RM-1543 (1955).

24. Herzberg, G., "Spectra of Diatomic Molecules," Second Edition, Van Nostrand, New York (1950).

25. Moore, C.E., National Bureau of Standards Circular 467, Vol. I (1949).

26. Weymann, H.D., Phys. of Fluids, 3, 545 (1960).

27. Wetzel, L.B., "On the Implications of Electron Diffusion through a Hypersonic Shock Front," Brown Univ. Sci. Rept. AF-4561/11, May 1961.

28. Townsend, J.S., Phil. Mag., 1, 198 (1901).

29. Loeb, L.B., "Basic Processes of Gaseous Electronics," Univ. of Calif. Press (1955).

30. Massey, H.S.W., and Burhop, E.H.S., "Electronic and Ionic Impact Phenomena," Oxford (1952).

31. Lin, S.C., Phys. Fluids, 4, 1277 (1961).

32. Tate, J.T., and Smith, P.T., Phys. Rev. 39, 270 (1932).

33. Weissler, G.L., Lee, Po., and Mohr, E.I., J. Opt. Soc. Am., 42, 84, 200 (1952); 45, 703 (1955); N. Wainfan, W.C. Walker and G.L. Weissler, J. Appl. Phys., 24, 1318 (1953); Phys. Rev., 99, 542 (1955); H. Sun and G.L. Weissler, J. Chem. Phys., 23, 1160 (1955).

34. Weissler, G. L., "Handbuck der Physik," (S. Flügge, ed.) Springer - Verlag, Berlin (1956), Vol. 21, p. 309.

35. Camm, J., Kivel, B., Taylor, R. L., and Teare, J. D., J. Quant. Spectrosc. Radiat. Transfer, 1, 53 (1962).

36. Teare, J. D., Georgiev, S. and Allen, R. A., "Radiation from the Non-equilibrium Shock Front," Avco-Everett Research Laboratory Research Report 112 (1961); also, Progress in Astronautics and Rocketry, Vol. 7 (F. Riddell, ed.), Academic Press, New York (1962), p. 281.

37. Hammerling, P., "Ionization Effects of Precursor Radiation from Shocks in Air," Avco-Everett Research Laboratory Research Report 98 (1960).

38. Brown, S. C., "Basic Data of Plasma Physics," M. I. T., John Wiley and Sons, New York (1959).

39. Massey, H. S. W., "Negative Ions," Cambridge Univ. Press (1950).

40. Branscomb, L. M., Burch, D. S., Smith, S. J., and Geltman, S., Phys. Rev. 111, 505 (1958).

41. Phelps, A. V., Pack, J. L., Phys. Rev. Letters, 6, 111 (1961).

42. Mitra, S. K., "The Upper Atmosphere," The Asiatic Society, Calcutta (1952).

43. Massey, H. S. W., and Burhop, E. H. S., Loc. cit., Chapt. VII, §10 and §11; N. F. Mott and H. S. W. Massey, "The Theory of Atomic Collisions," Oxford (1952), Chapt. VIII.

44. Lin, S. C., "Ionization Phenomenon of Shock Waves in Oxygen-Nitrogen Mixtures," Avco-Everett Research Laboratory, Research Report 33 (1958).

45. Bates, D. R. and Massey, H. S. W., Phil. Mag. Series 7, 45, 111 (1954).

46. Bransden, B. H. and Dalgarno, A., Proc. Phys. Soc. A, 66, 904 and 911 (1953).

47. Wu, T. Y., Phys. Rev. 66, 291 (1944).

48. Chapman, S. and Cowling, T. G., "The Mathematical Theory of Non-Uniform Gases," Cambridge Univ. Press, N. Y. (1952) p. 93.

49. Doering, J. P. and Mahan, B. H., "The Vacuum Ultraviolet Photolysis of Nitrous and Nitric Oxide," Chemical Reactions in the Lower and Upper Atmosphere, Interscience, N. Y. (1961).

50. Kasner, W. H., Rogers, W. A. and Biondi, M. A., Bull. Am. Phys. Soc., Series II, 7, 131 (1962).

51. Utterback, N. G. and Miller, G. H., Phys. Rev. 124, 1477 (1961).

52. Utterback, N. G., Bull. Am. Phys. Soc., Series II, 7, 487 (1962).

53. Utterback, N. G., "Ionization of Nitrogen and Oxygen Molecules by Nitrogen and Oxygen Molecules," (to be published in the Physical Review).

54. Eschenroeder, A. Q., American Rocket Society Jour., 32, 196 (1962).

55. Thomson, J. J., Phil. Mag. 47, 337 (1924).

56. Lin, S. C., J. Geophys. Res., 67, 3851 (1962).

57. Spitzer, L., Jr., "Physics of Fully Ionized Gases," Interscience, N. Y. (1956) p. 17.

58. Shkarofsky, I. P., Bachynski, M. P. and Johnston, T. W., Planetary and Space Science, 6, 24 (1961).

59. Liepmann, H. W. and Roshko, A., "Elements of Gasdynamics," John Wiley and Sons, N. Y. (1957) p. 85.

60. Gibson, W. E. and Marrone, P. V., "A Correspondence Between Normal Shock and Blunt-Body Flows," Cornell Aero. Lab., Report No. 253-62 (1962).

61. Eschenroeder, A. Q., Daiber, J. W., Golian, T. C. and Hertzberg, A., "Shock Tunnel Studies of High-Enthalpy Ionized Airflows," Cornell Aero. Lab., Report No. AF-1500-A-1 (1962).

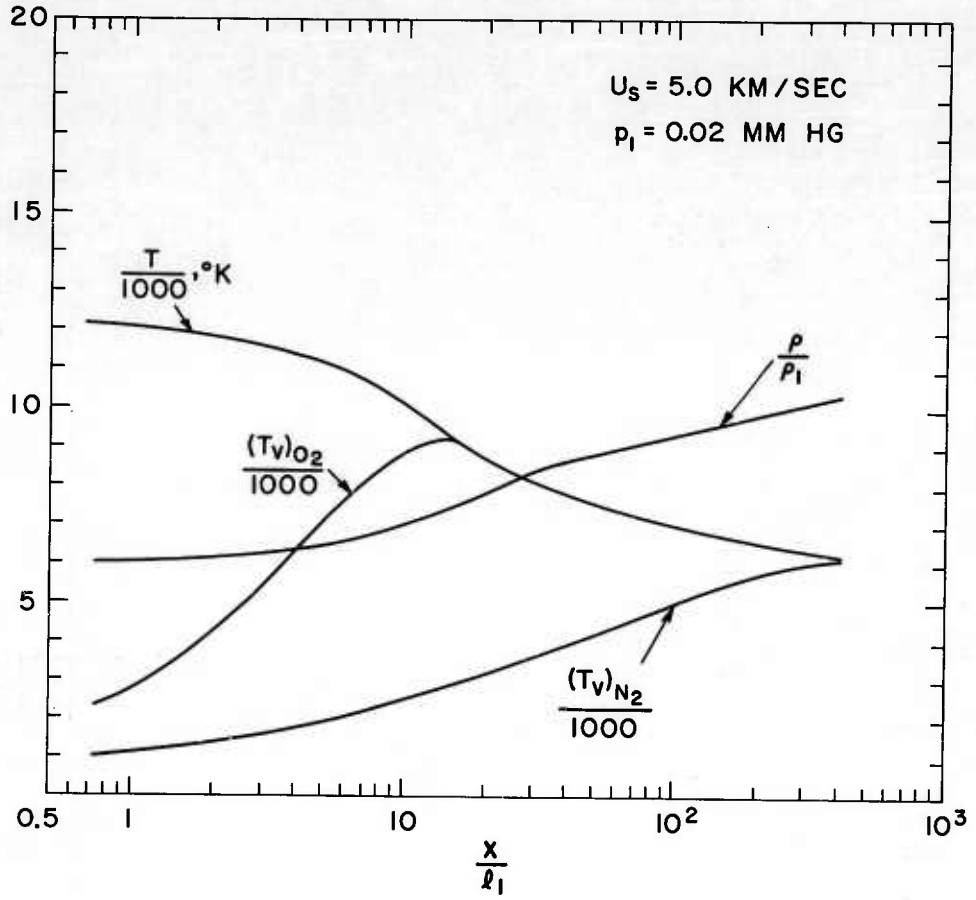

Fig. 1 (a) Typical temperature and density distribution behind a normal shock wave in air calculated from coupled vibrational excitation and chemical reactions. x/ℓ_1 is the distance behind the translational/rotational shock front divided by the upstream mean free path.

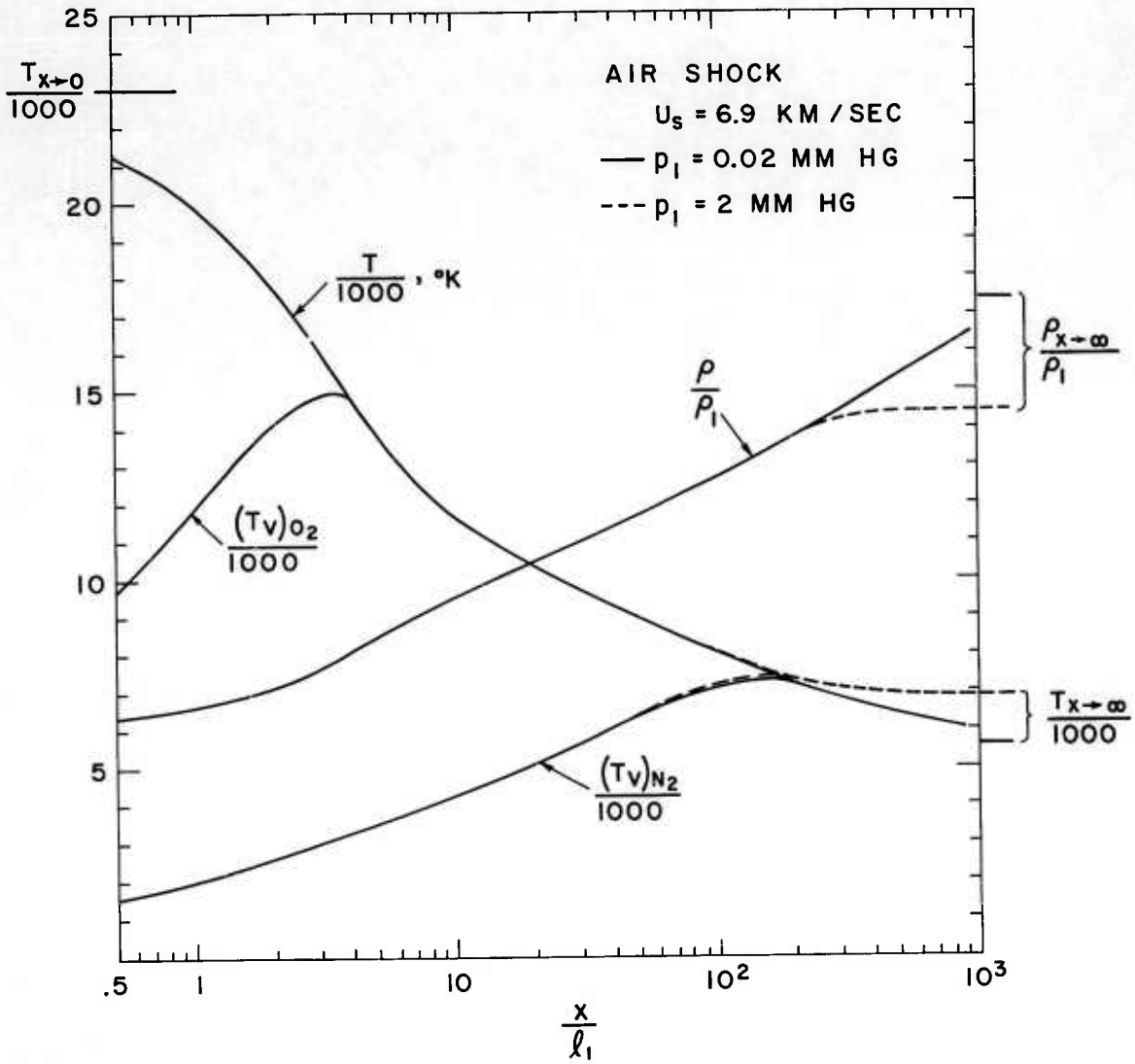

Fig. 1 (b) Typical temperature and density distribution behind a normal shock wave in air calculated from coupled vibrational excitation and chemical reactions. x/ℓ_1 is the distance behind the translational/rotational shock front divided by the upstream mean free path.

8817

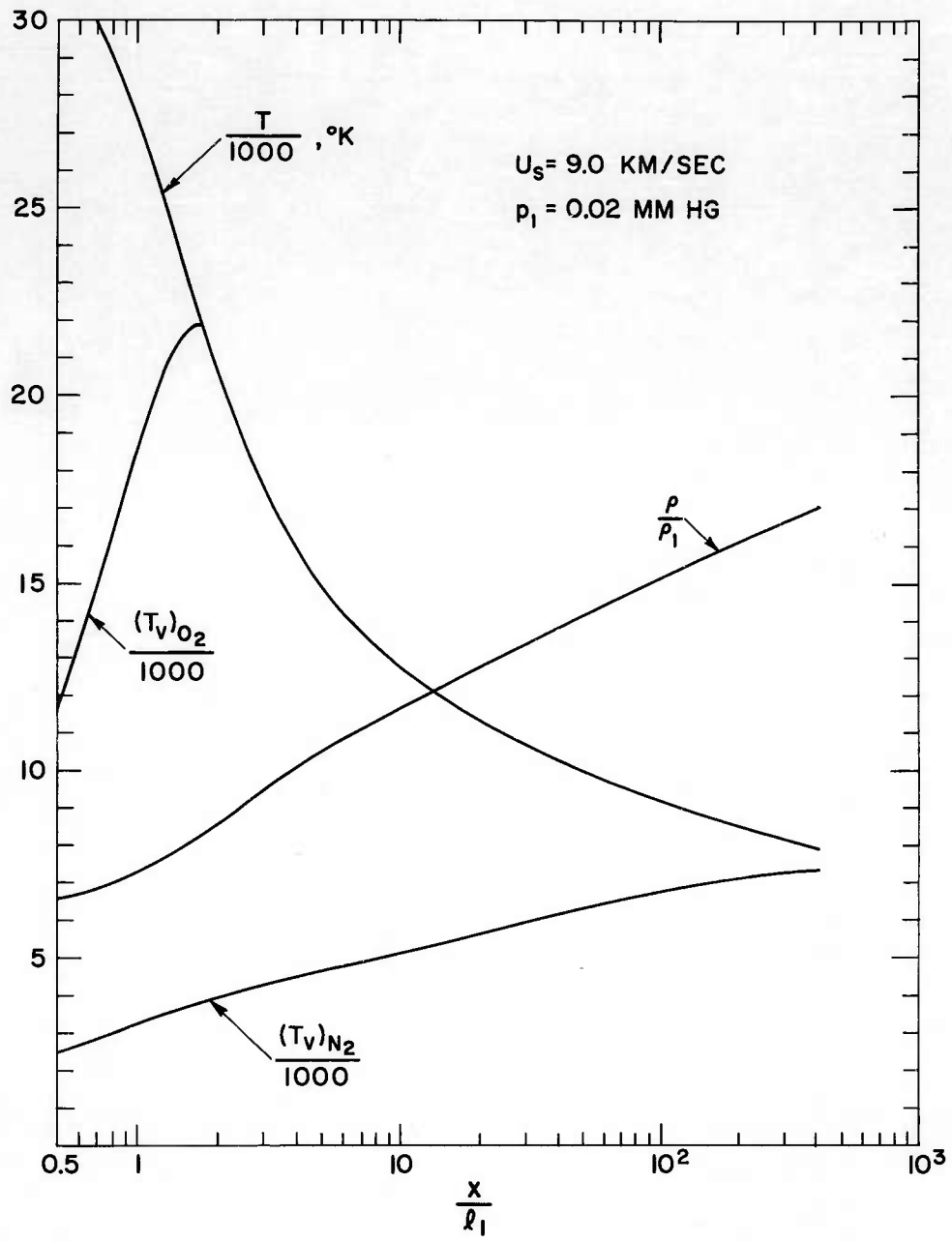

Fig. 1 (c) Typical temperature and density distribution behind a normal shock wave in air calculated from coupled vibrational excitation and chemical reactions. x/ℓ_1 is the distance behind the translational/rotational shock front divided by the upstream mean free path.

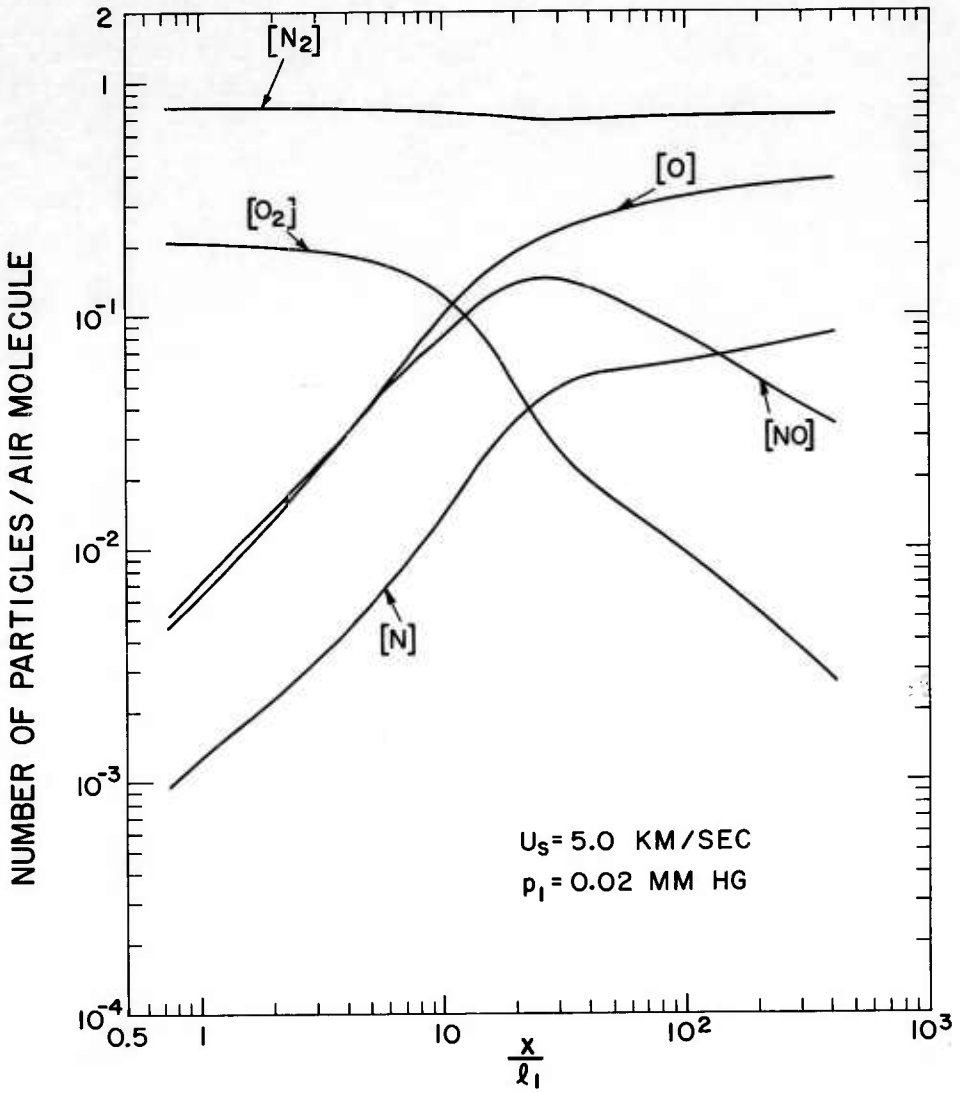

Fig. 2 (a) Typical neutral particle distribution behind a normal shock wave in air calculated from coupled vibrational excitation and chemical reactions. [X] is the total number of type X particles at all internal energy states per unit volume divided by the equivalent number of air molecules within the same volume.

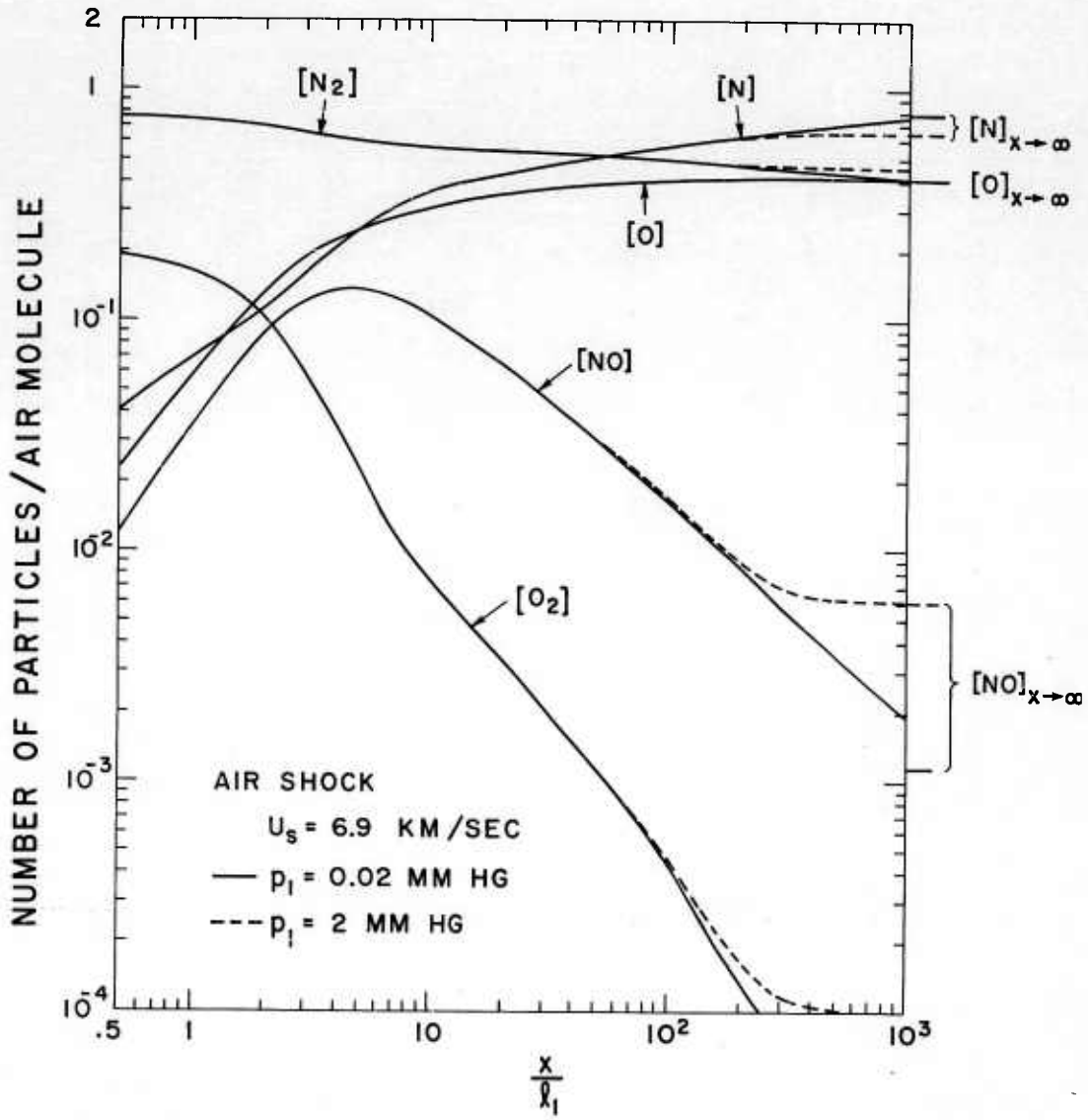

Fig. 2 (b) Typical neutral particle distribution behind a normal shock wave in air calculated from coupled vibrational excitation and chemical reactions. [X] is the total number of type X particles at all internal energy states per unit volume divided by the equivalent number of air molecules within the same volume.

8818

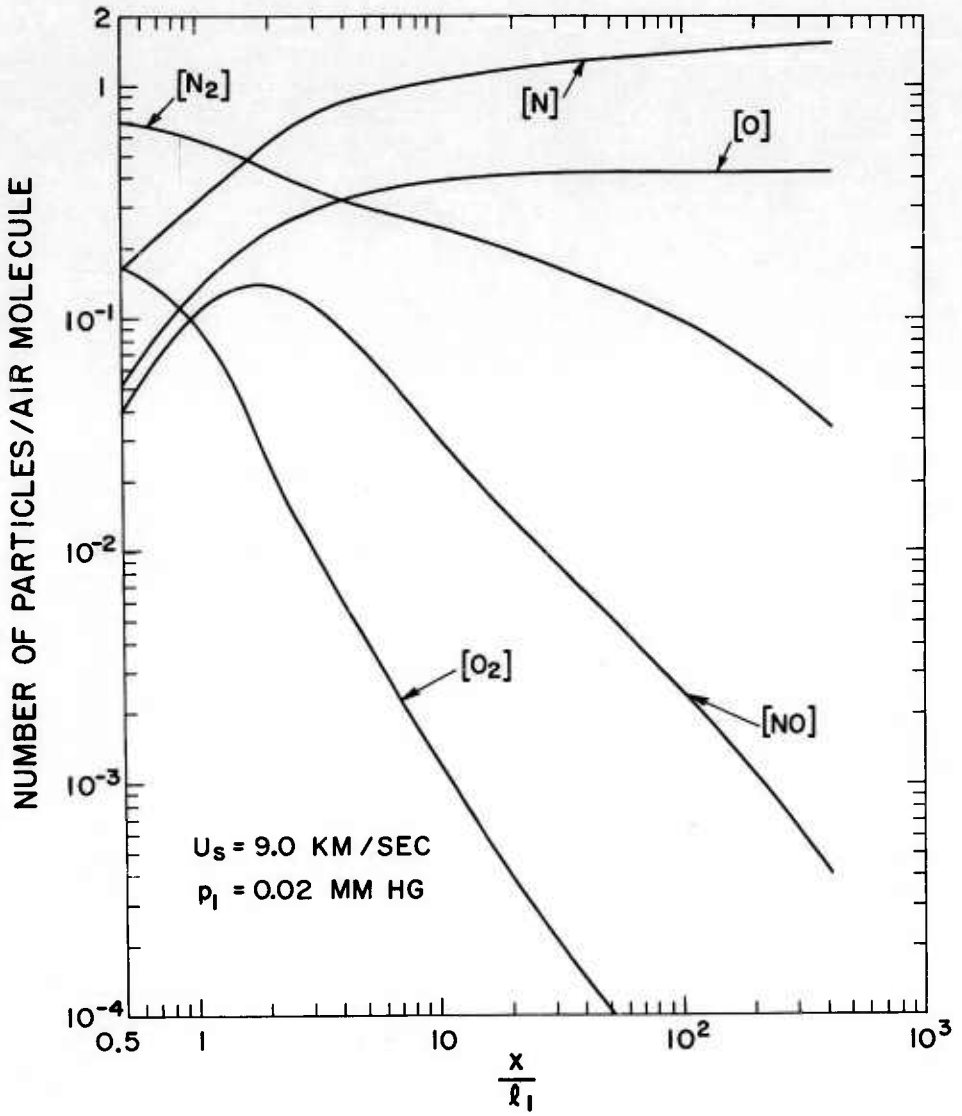

Fig. 2 (c) Typical neutral particle distribution behind a normal shock wave in air calculated from coupled vibrational excitation and chemical reactions. [X] is the total number of type X particles at all internal energy states per unit volume divided by the equivalent number of air molecules within the same volume.

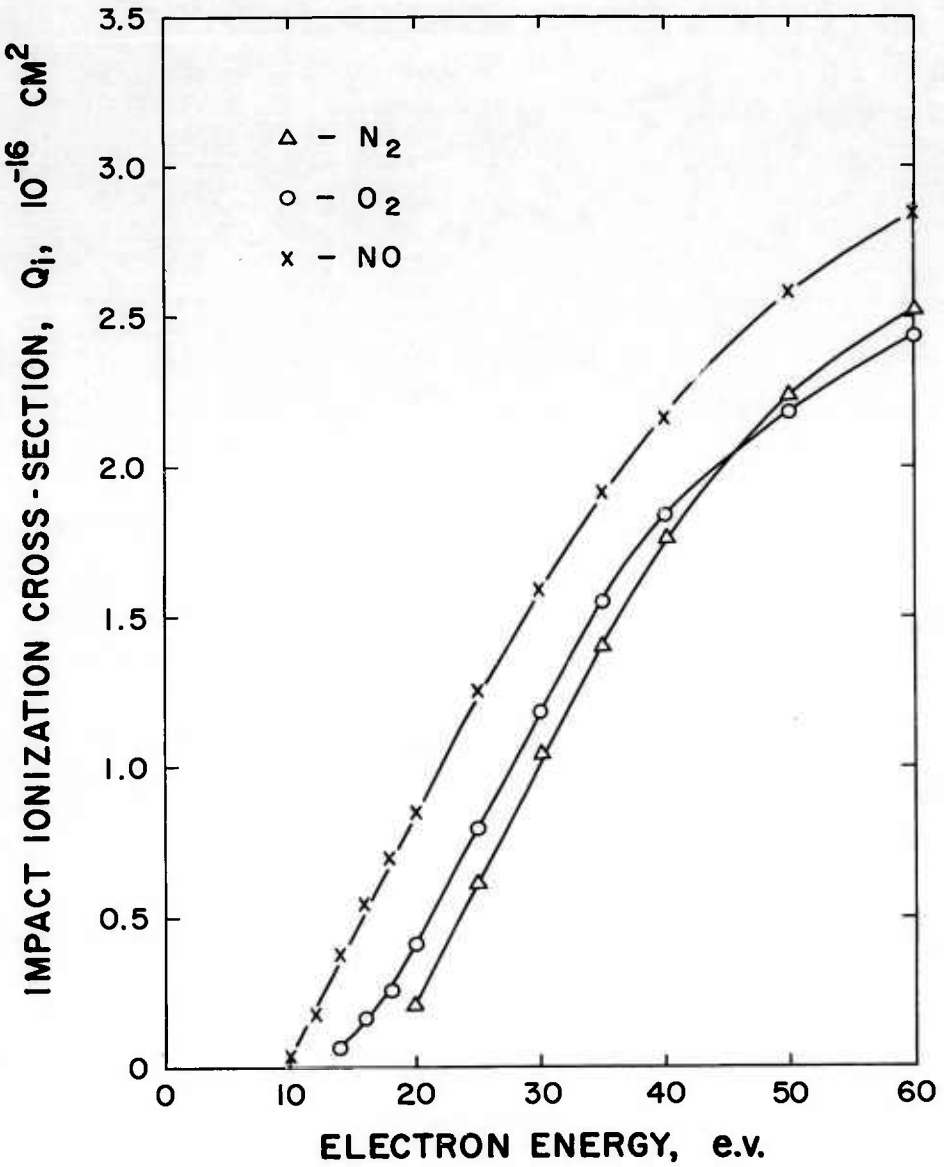

Fig. 3 Apparent total ionization cross-sections for N_2, O_2 and NO by electron impact according to Tate and Smith (Refs. 30 and 32).

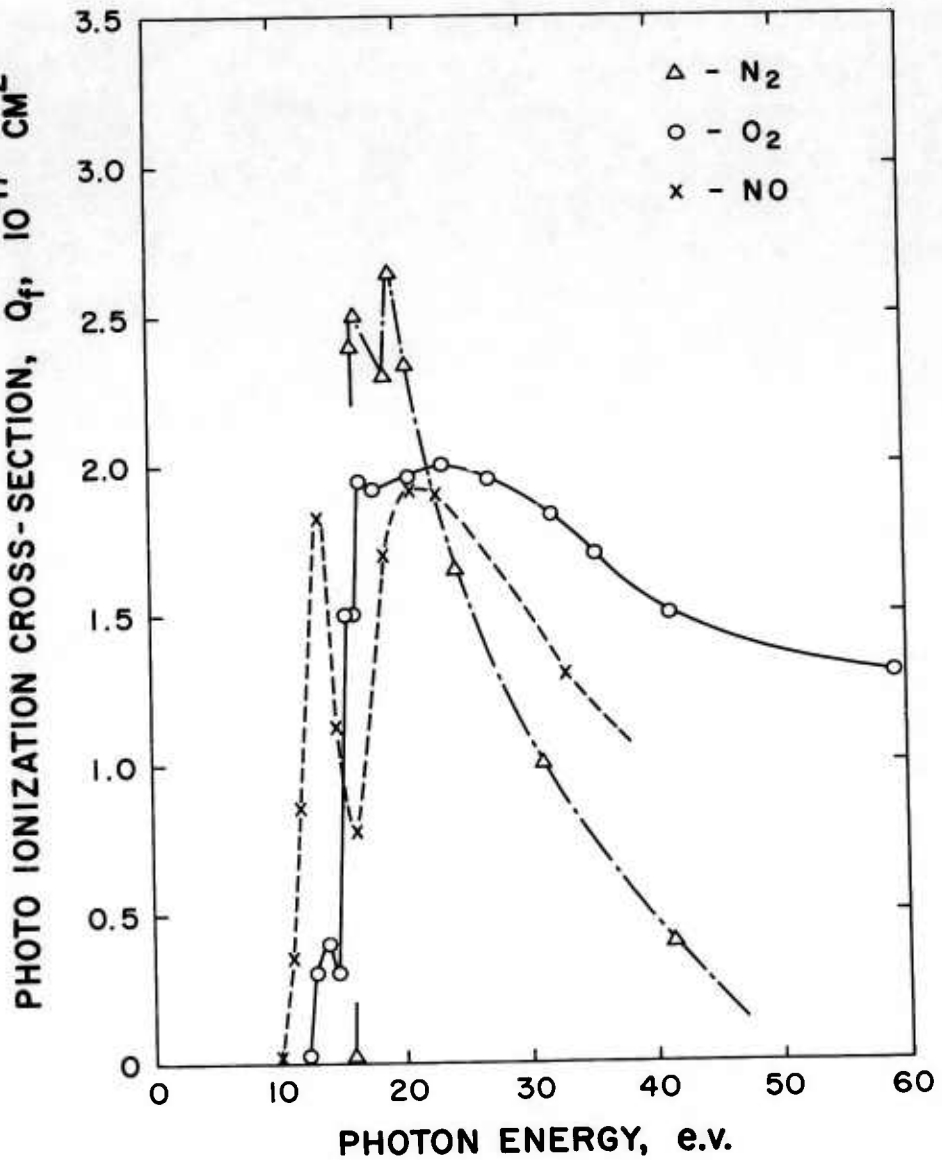

Fig. 4 Photoionization cross-sections for N_2, O_2 and NO according to Weissler et al (Refs. 33 and 34).

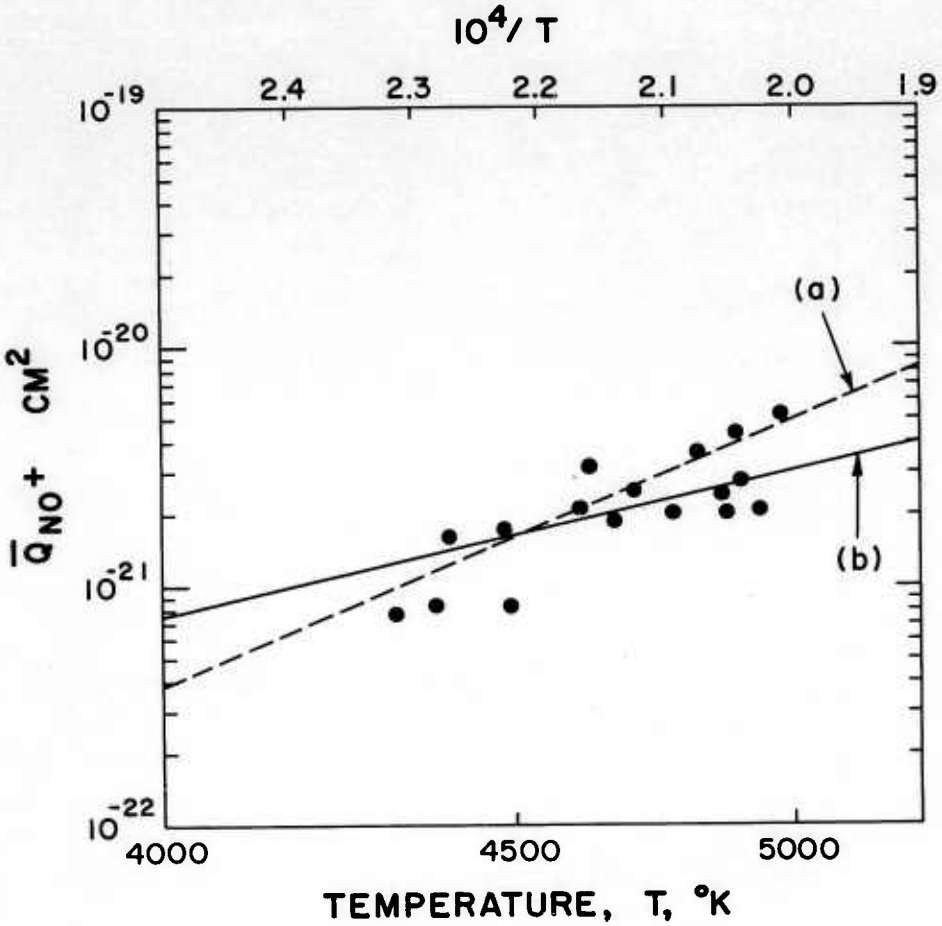

Fig. 5 Velocity-averaged ionization cross-section for N-O collisions deduced from observation of the ionization rate behind shock waves in gas mixtures containing a small percentage of O_2 in N_2 (Ref. 44). Note that a correction factor of about 5 has been applied to the previous lower bound estimate to allow for the finite dissociation rates of O_2 and N_2 (see footnote on page 24).

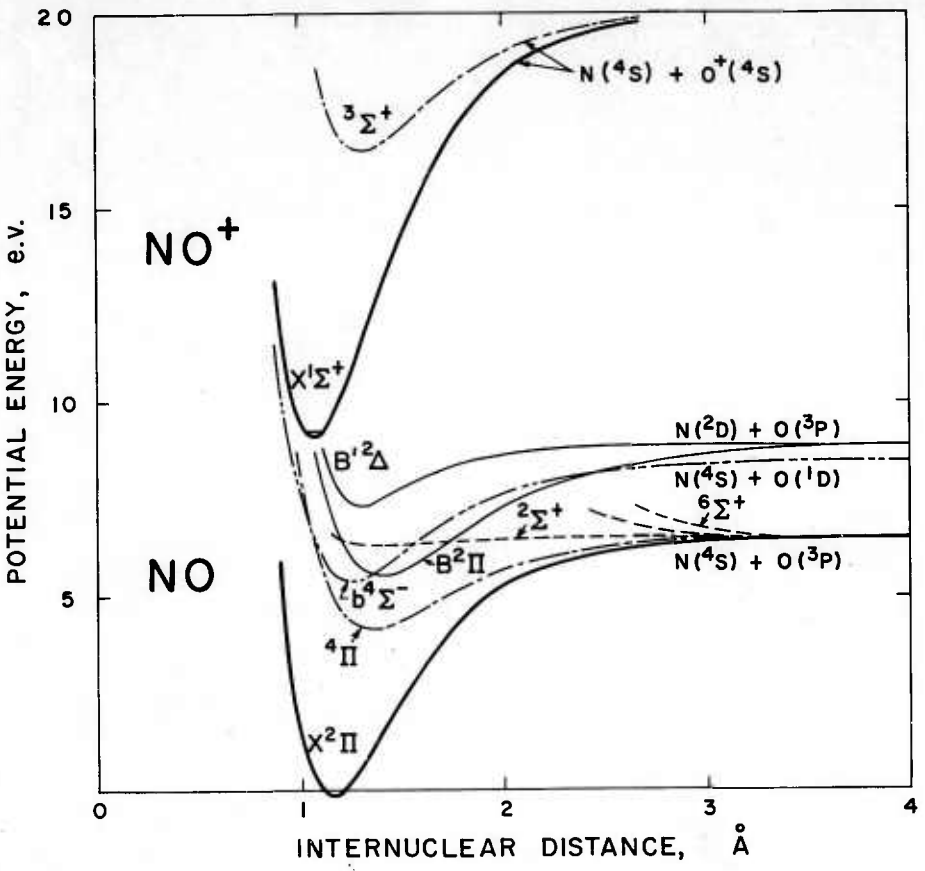

Fig. 6 Potential energy curves for the lower electronic states of the NO and the NO^+ systems. (Courtesy F. R. Gilmore, Rand Corp.)

8822

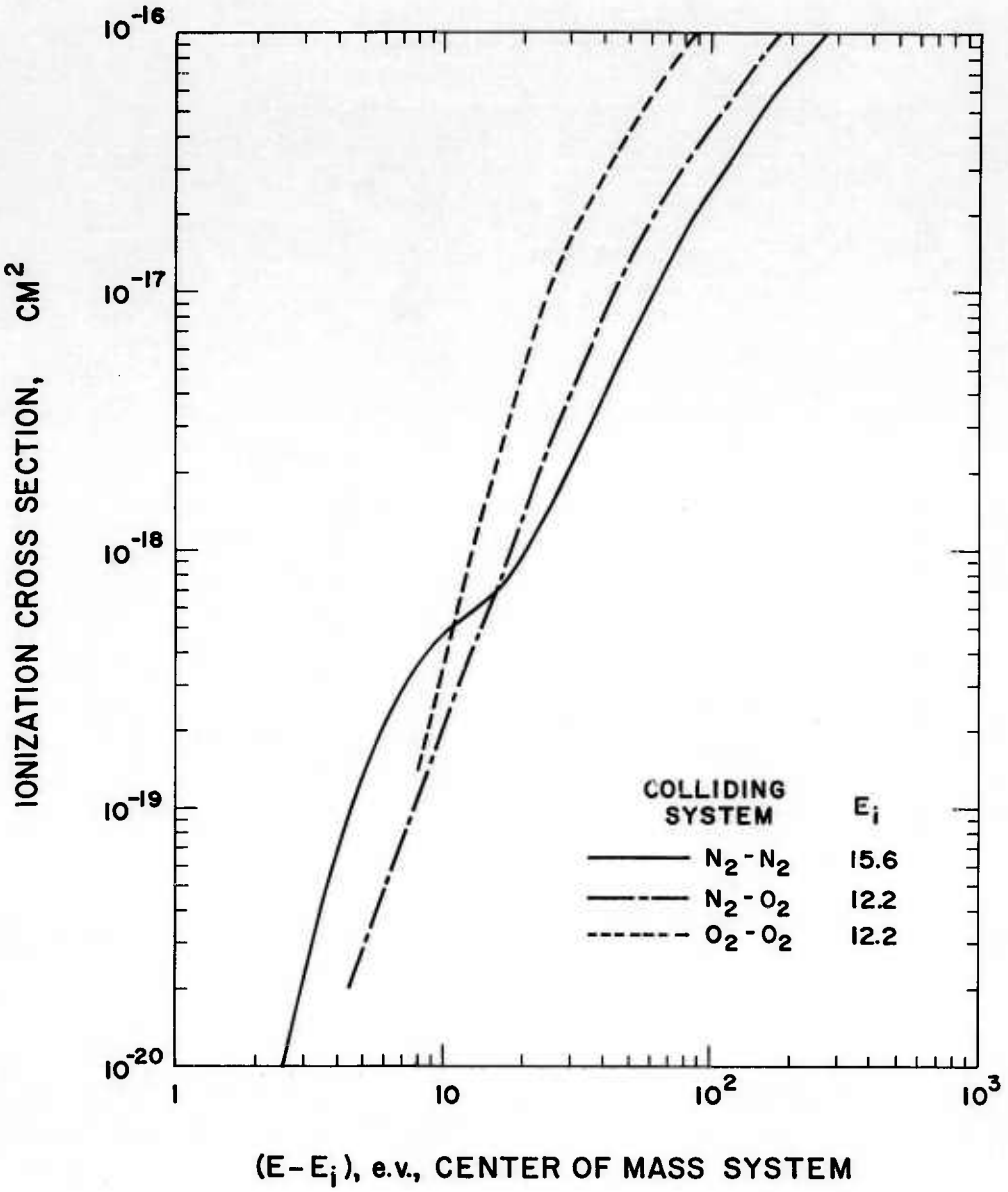

Fig. 7 Ionization cross-sections for N_2-N_2, N_2-O_2 and O_2-O_2 collisions obtained from molecular beam experiments by Utterback and Miller (Ref. 51) and by Utterback (Refs. 52 and 53).

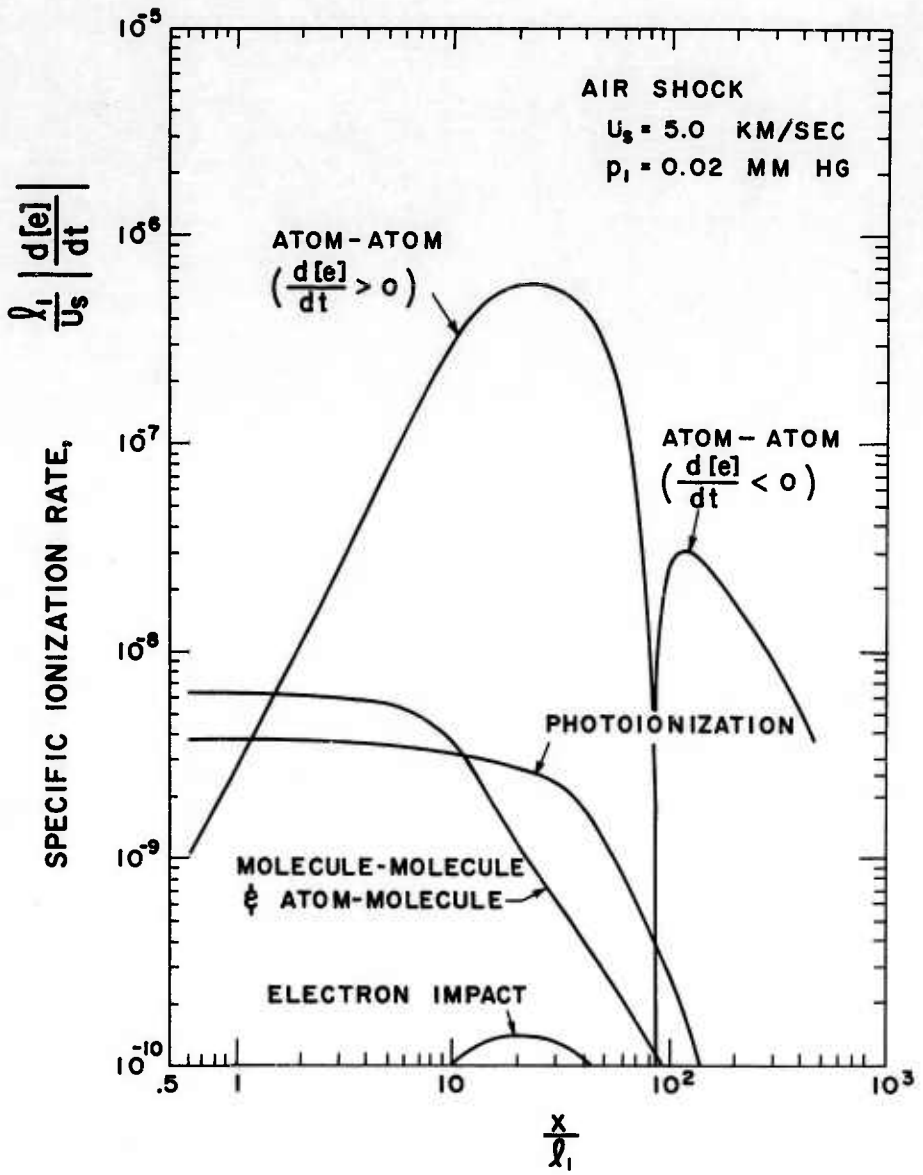

Fig. 8 (a) Specific ionization rates for the various groups of ionization processes as functions of distance behind the shock at U_s = 5.0 km/sec and p_1 = 0.02 mm Hg.

8824

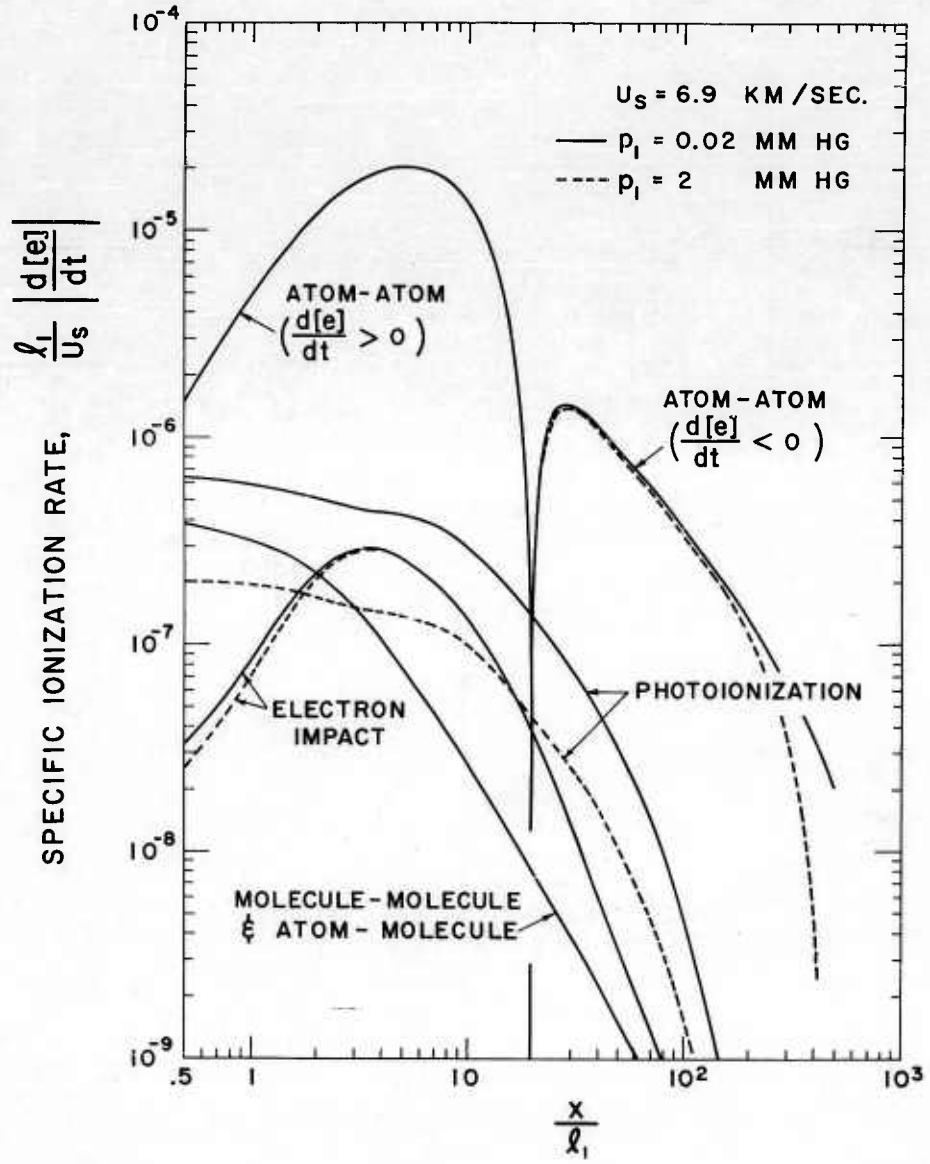

Fig. 8 (b) Specific ionization rates for the various groups of ionization processes as functions of distance behind the shock at U_s = 6.9 km/sec and at two different values of the initial pressure p_1.

8825

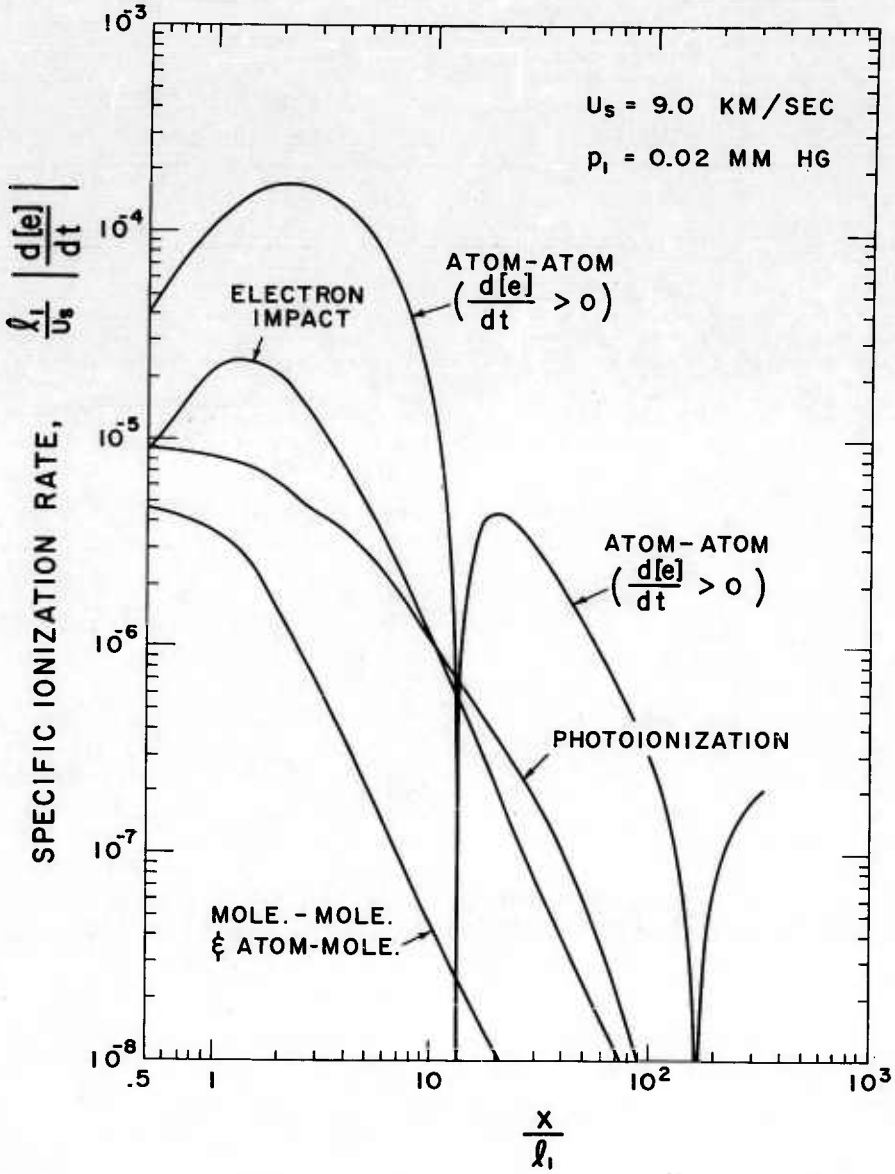

Fig. 8 (c) Specific ionization rates for the various groups of ionization processes as functions of distance behind the shock at U_s = 9.0 km/sec and p_1 = 0.02 mm Hg.

8828

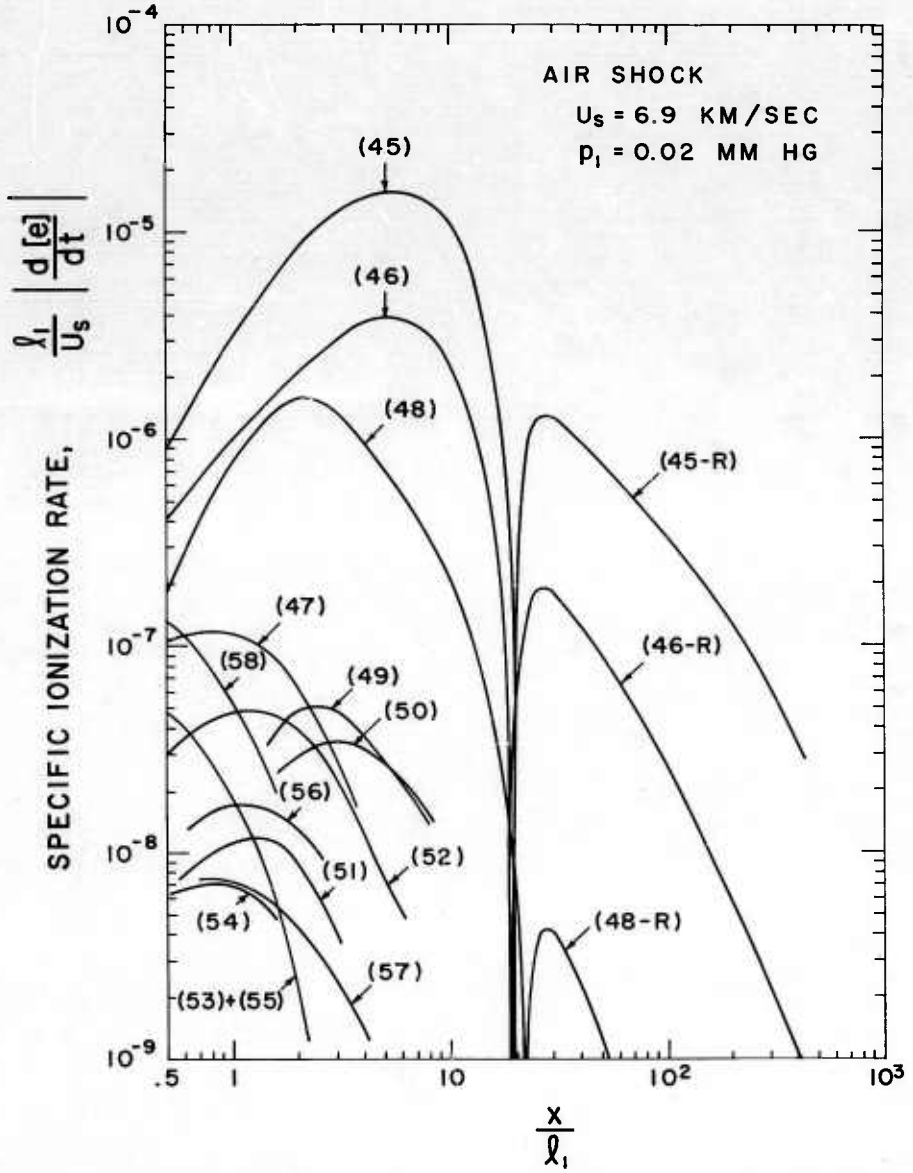

Fig. 9 Detail breakdown of specific ionization rates for the various atom-atom, atom-molecule and molecule-molecule reactions as functions of distance behind the shock for the case U_s = 6.9 km/sec and p_1 = 0.02 mm Hg. The curves labelled (45-R), (46-R) and (48-R) indicate negative electron production rate due to the excess of the backward rate over the forward rate for reactions (45), (46) and (48) respectively.

8827

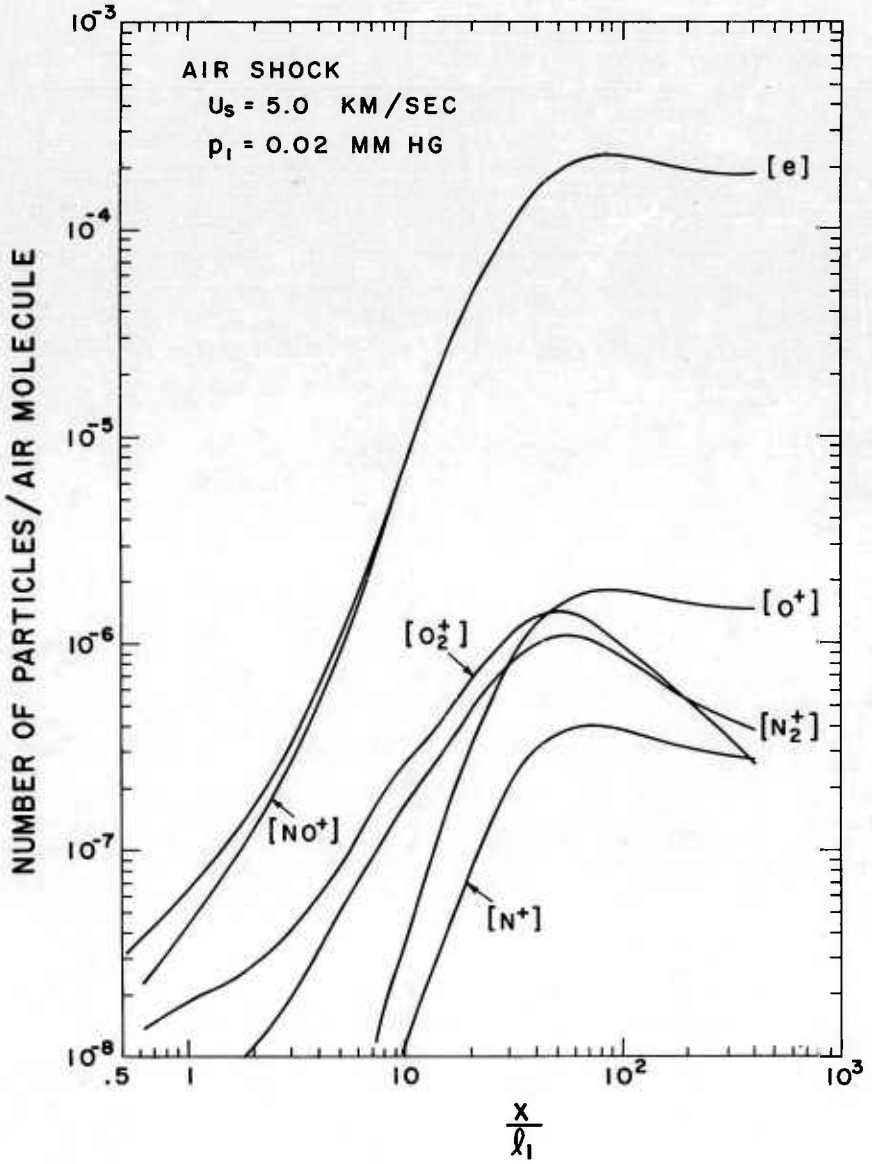

Fig. 10 (a) Distribution of free electrons and various positive ions behind the shock at U_s = 5.0 km/sec and p_1 = 0.02 mm Hg. These results are obtained by integration of the resultant net production rate of the corresponding species due to the various ionization processes. The effects of diffusion and upstream photoionization have been neglected, but charge exchange reactions are allowed to proceed simultaneously with the production processes, assuming a universal exothermic charge exchange cross-section of $3\pi a_o^2$.

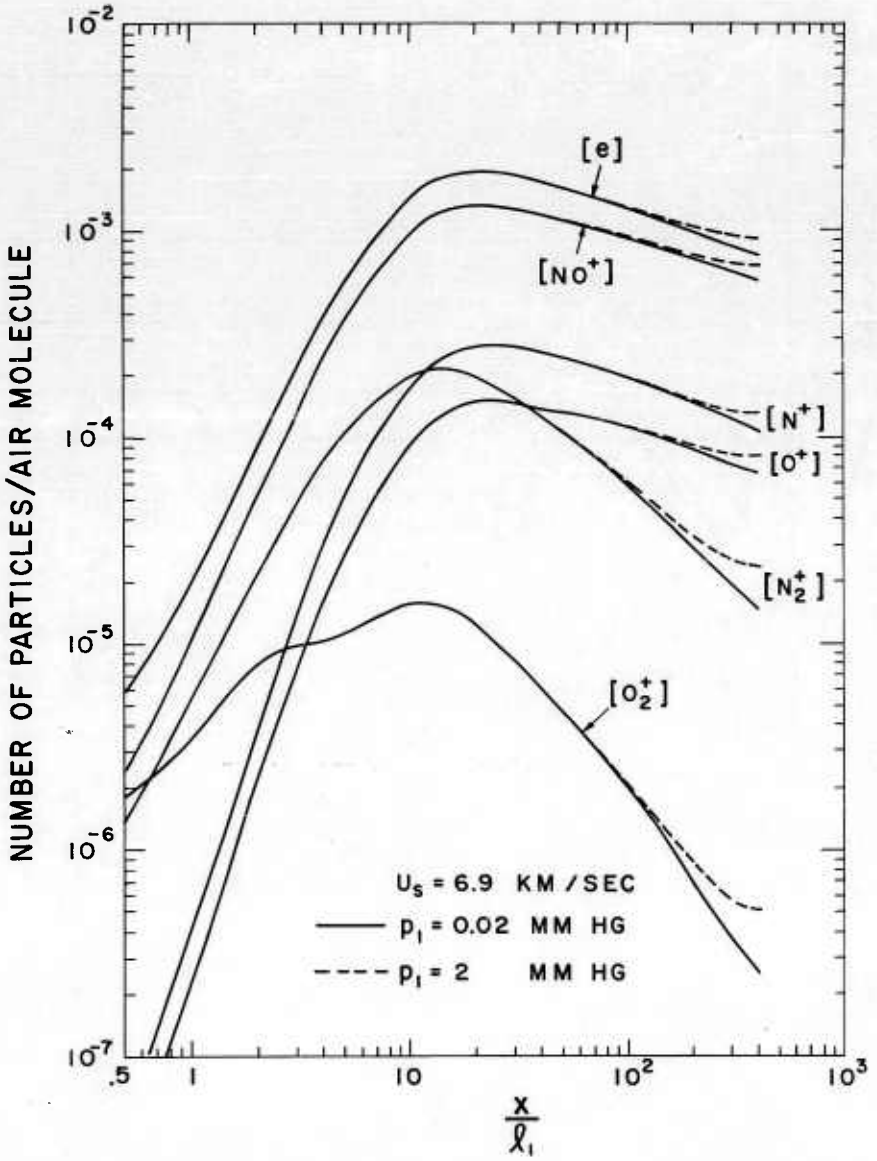

Fig. 10 (b) Distribution of free electrons and various positive ions behind the shock at U_s = 6.9 km/sec and at two different values of the initial pressure p_1. These results are obtained by integration of the resultant net production rate of the corresponding species due to the various ionization processes. The effects of diffusion and upstream photo-ionization have been neglected, but charge exchange reactions are allowed to proceed simultaneously with the production processes, assuming a universal exothermic charge exchange cross-section of $3\pi\, a_o^2$.

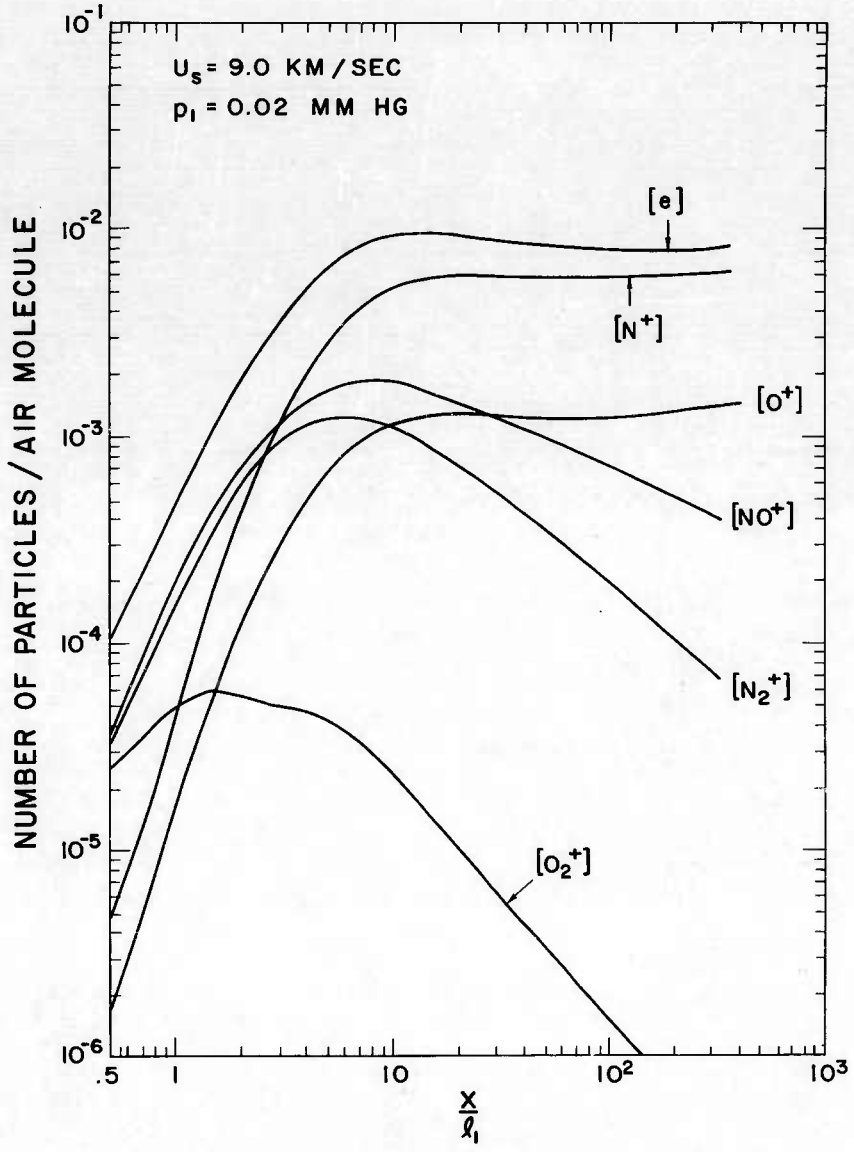

Fig. 10 (c) Distribution of free electrons and various positive ions behind the shock at U_s = 9.0 km/sec and p_1 = 0.02 mm Hg. These results are obtained by integration of the resultant net production rate of the corresponding species due to the various ionization processes. The effects of diffusion and upstream photoionization have been neglected, but charge exchange reactions are allowed to proceed simultaneously with the production processes, assuming a universal exothermic charge exchange cross-section of $3\pi a_o^2$.

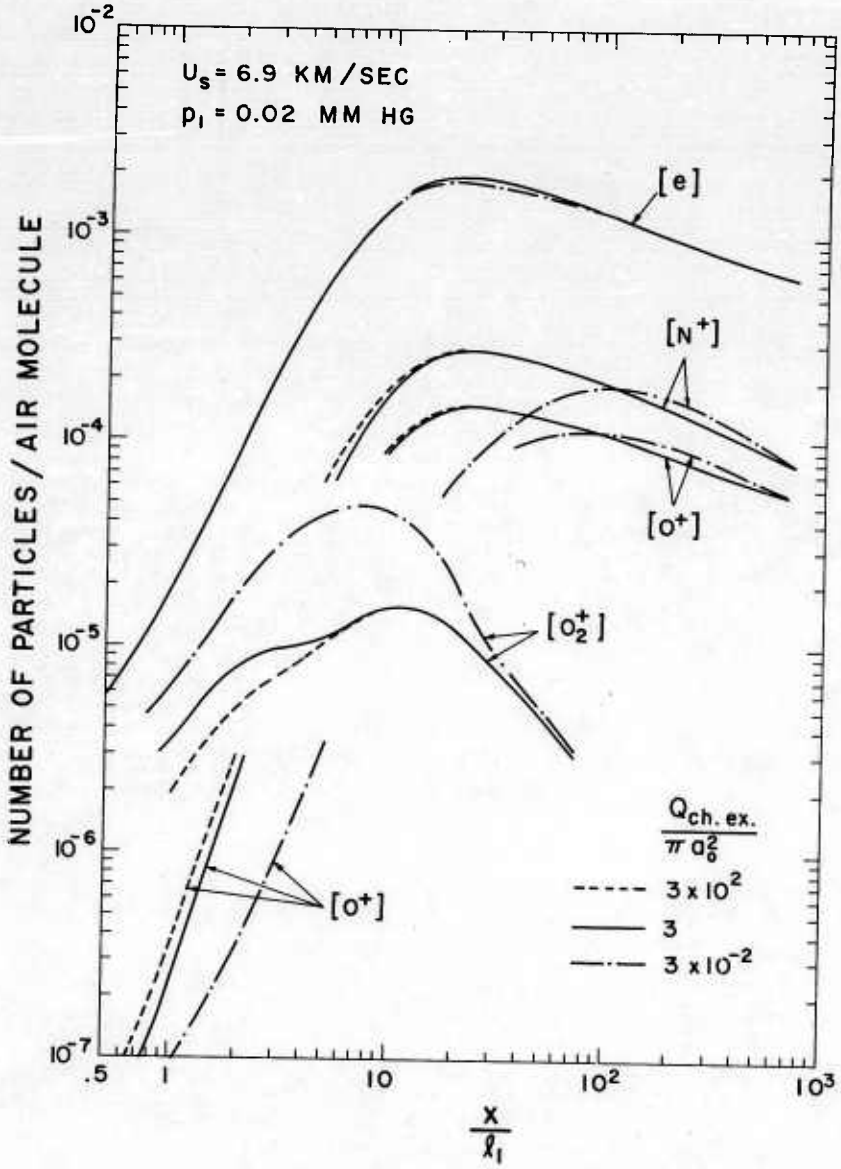

Fig. 11 Effects of varying the universal exothermic charge exchange cross-section by a factor of 100 in either direction on the distributions of free electrons and N^+, O^+ and O_2^+ ions behind the shock for the case U_s = 6.9 km/sec and p_1 = 0.02 mm Hg. The corresponding effects on the distribution of NO^+ and N_2^+ ions not shown are between those of the electrons and of the other three positive ions.

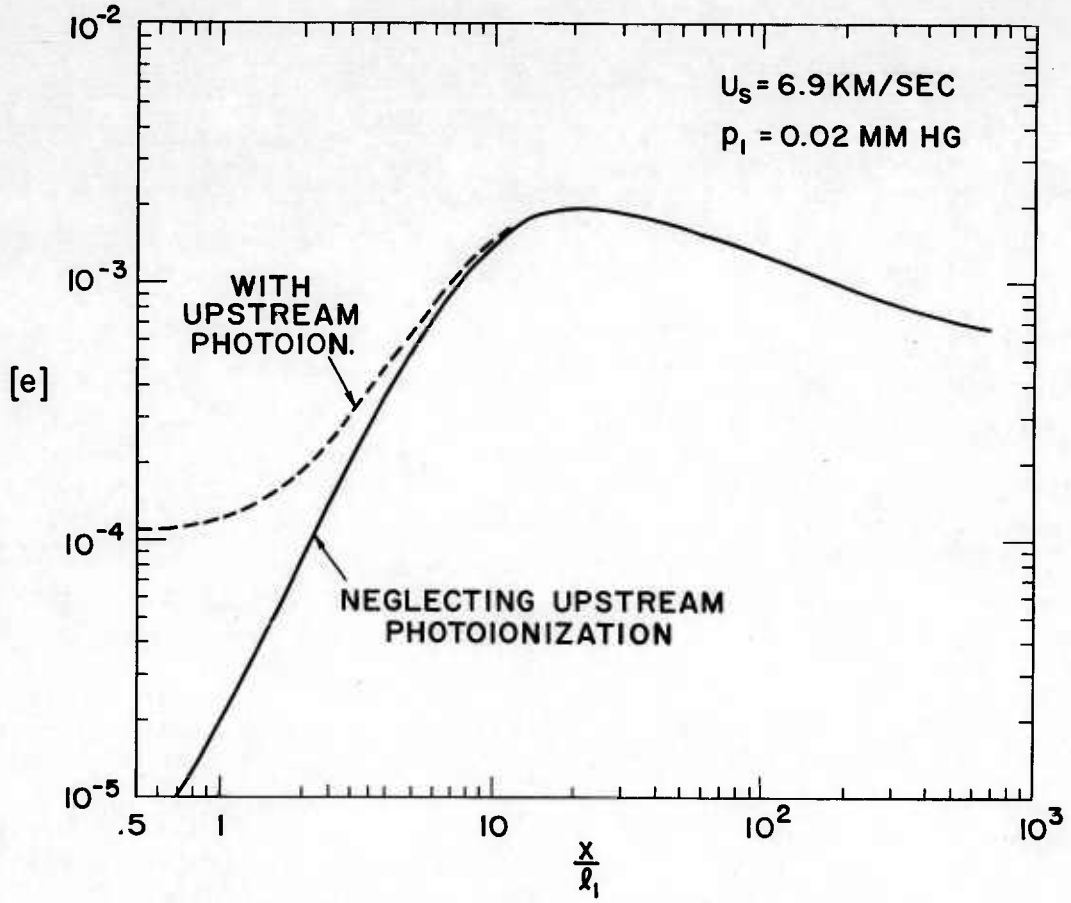

Fig. 12 Effect of inclusion of upstream photoionization on the distribution of free electrons behind the shock for the case U_s = 6.9 km/sec and p_1 = 0.02 mm Hg.

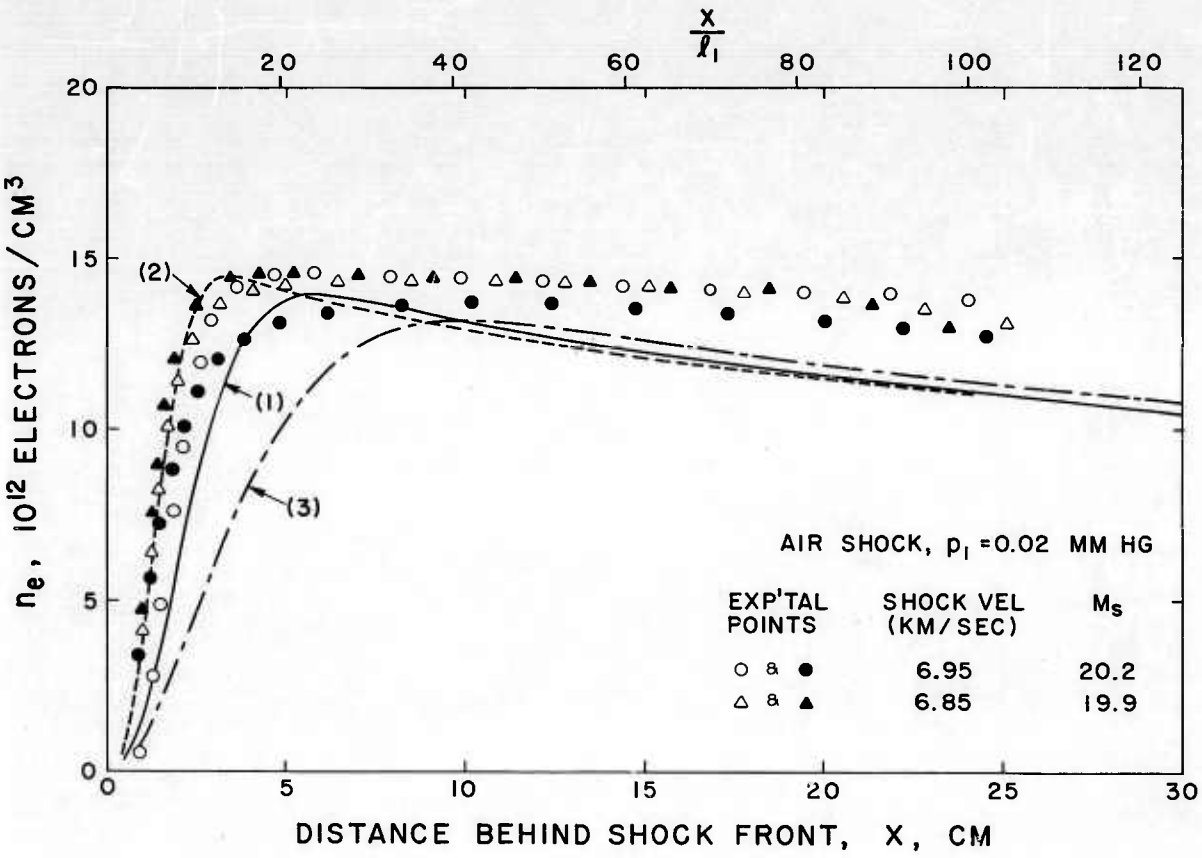

Fig. 13 Comparison between calculated and observed electron density distributions behind the shock for the case $U_s = 6.9 \pm 0.05$ km/sec and $p_1 = 0.02$ mm Hg. The theoretical curve (1) is based on the adopted set of rate constants described in Section IV, and the curves (2) and (3) are obtained by varying the predominant ionization rate constant κ_{45} by a factor of 3 in either directions while keeping all other rate constants the same. Upstream photoionization has not been included in the theoretical curves since its effect is smaller than the experimental scatter.

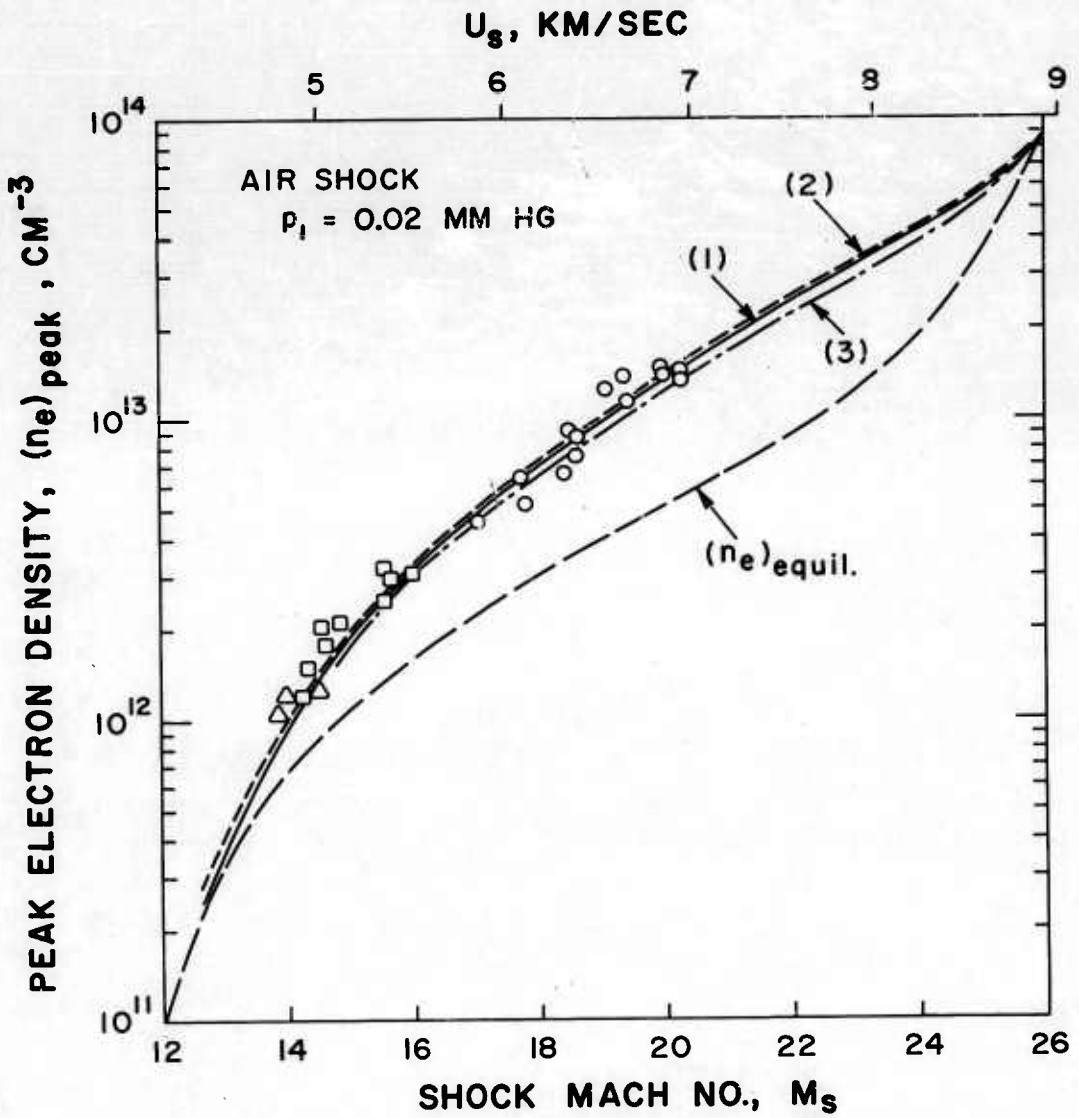

Fig. 14 Comparison between calculated and observed peak electron density behind the shock as a function of shock velocity at p_1 = 0.02 mm Hg. The theoretical curves (1), (2) and (3) have the same meaning as in Fig. 13. The curve $(n_e)_{equil.}$ gives the theoretical electron density corresponding to the final adiabatic equilibrium state far behind the shock. The experimental points are taken directly from Fig. 8 of Ref. 1.

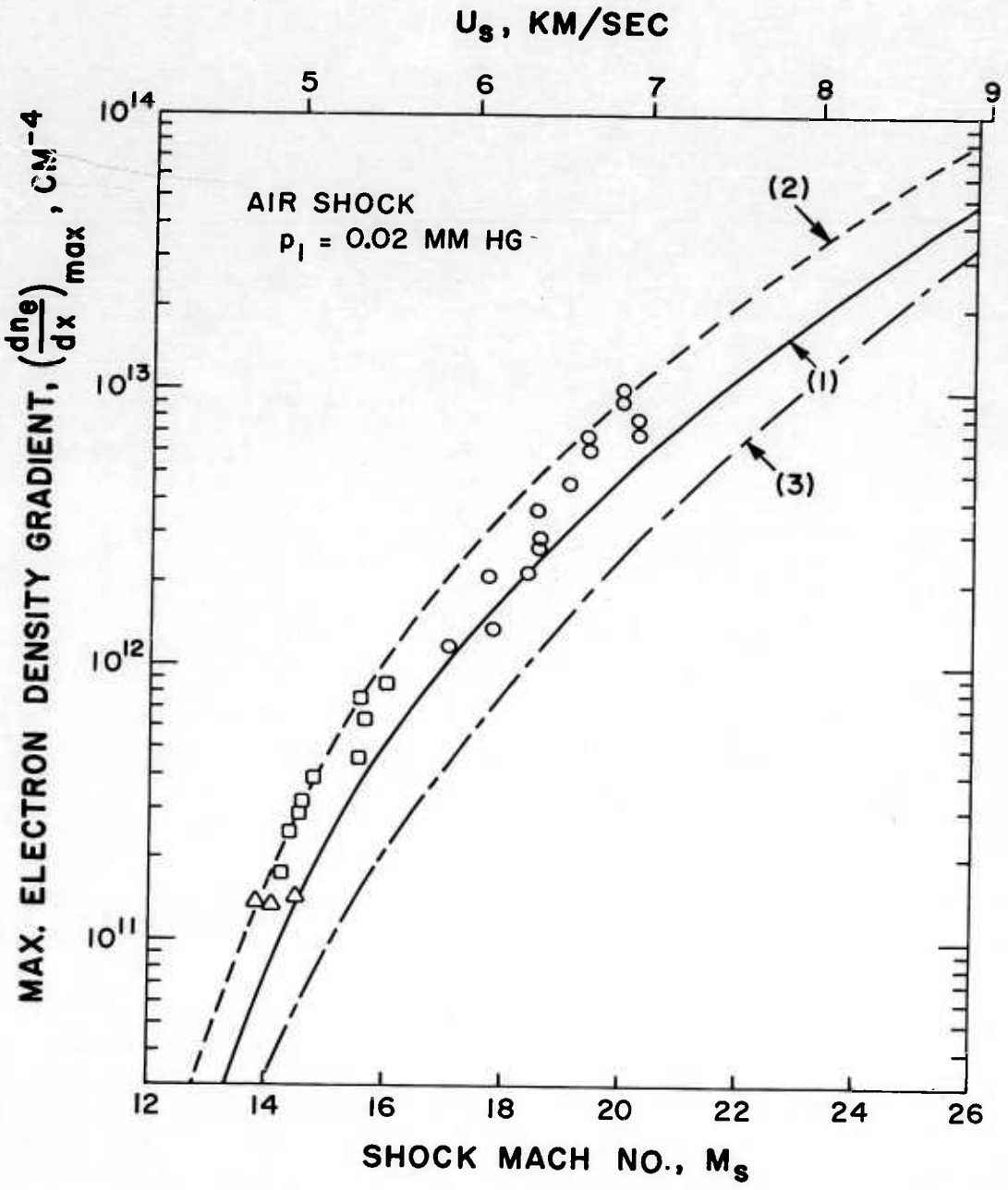

Fig. 15 Comparison between calculated and observed maximum electron density gradient behind the shock as a function of shock velocity at p_1 = 0.02 mm Hg. The theoretical curves (1), (2) and (3) have the same meaning as in Fig. 13. The experimental points are taken directly from Fig. 10 of Ref. 1.

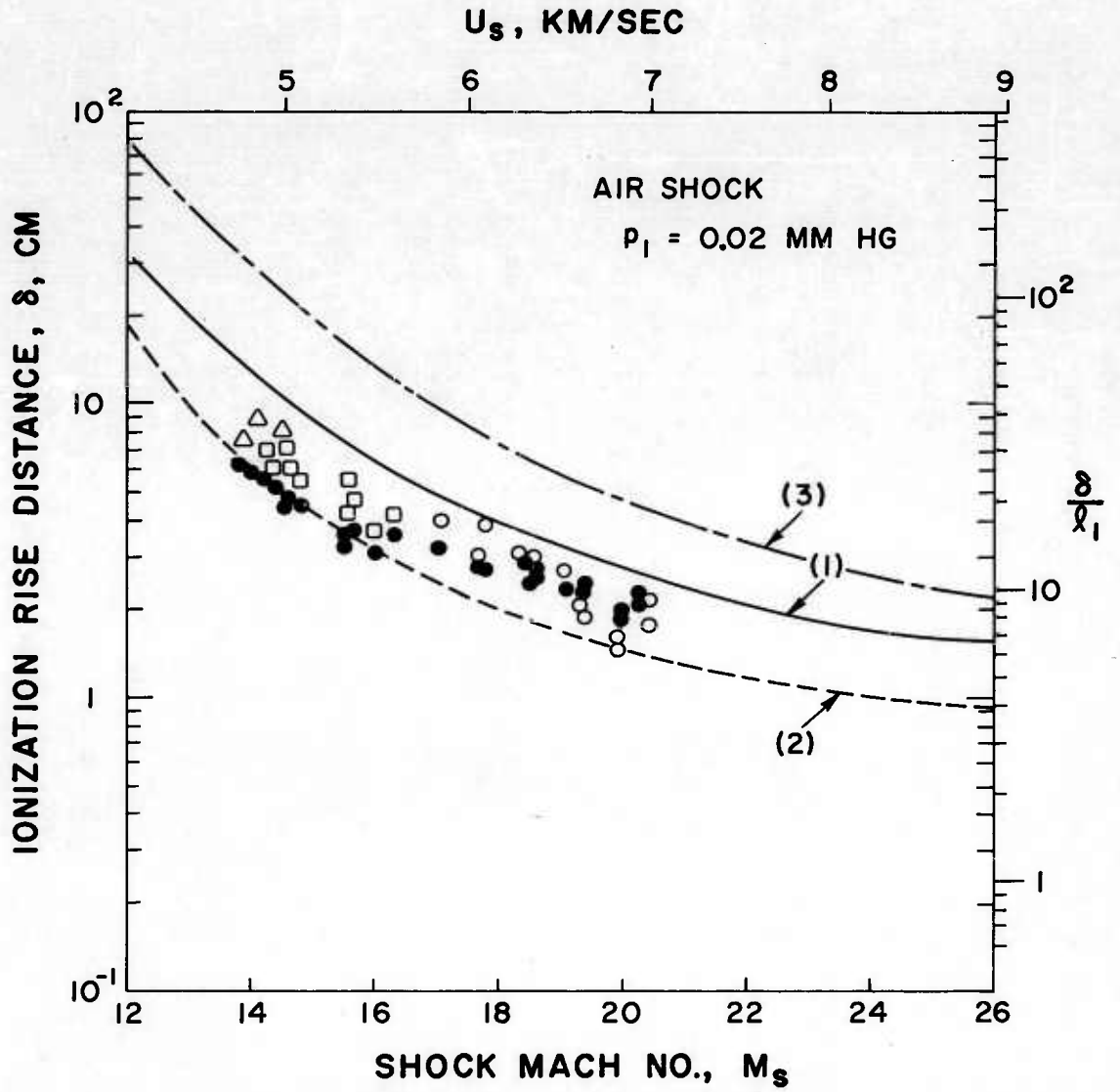

Fig. 16 Comparison between calculated and observed ionization rise distance behind the shock as a function of shock velocity at p_1 = 0.02 mm Hg. The theoretical curves (1), (2) and (3) have the same meaning as in Fig. 13. The experimental points are taken directly from Fig. 11 of Ref. 1.

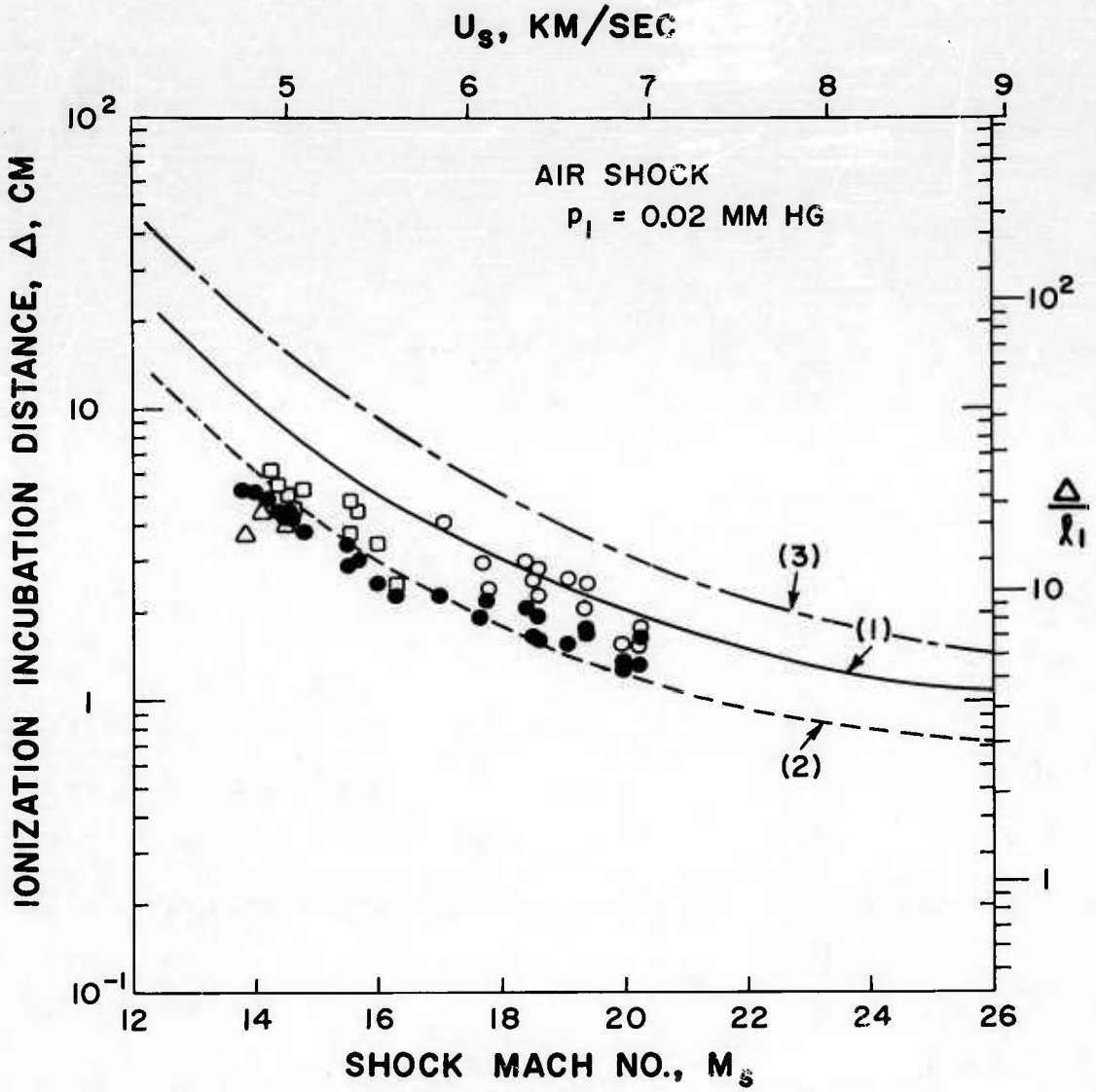

Fig. 17 Comparison between calculated and observed ionization incubation distance behind the shock as a function of shock velocity at p_1 = 0.02 mm Hg. The theoretical curves (1), (2) and (3) have the same meaning as in Fig. 13. The experimental points are taken directly from Fig. 12 of Ref. 1.

Avco-Everett Research Laboratory, Everett, Massachusetts
RATE OF IONIZATION BEHIND SHOCK WAVES IN AIR - II. THEORETICAL INTERPRETATION, by S. C. Lin and J. D. Teare. September 1962. 67 p. incl. illus. (Project 5561; Task 46308) (Avco-Everett Research Report 115; AFCRL - 62 - 751)
(Contract AF 19(604) - 7458)
Unclassified report

The problem of spontaneous ionization (i. e., no externally applied electromagnetic fields, nor hard radiation) in the reaction zone behind strong normal shock waves in air has been treated concurrently with the problem of dissociation and vibrational relaxation. Through a comparison of specific ionization rates, one may conclude that up to a shock velocity of 10 km/sec (about 30 times the speed of sound at room temperature) the predominant electron production process would be atom-atom ionizing collisions. This would be followed in an approximately decreasing order of importance by photo-ionization, electron impact, atom-molecule collisions and

(over)

molecule-molecule collisions. The charge exchange reactions, while not contributing directly to the electron production process, were found to have a small but noticeable indirect effect on the resultant electron density distribution at some distance behind the shock due to their continuous shifting of the relative population between atomic and molecular ions (which recombine with the electrons at different rates). The specific rate constants for the atom-atom processes required to interpret all existing experimental results appear to be consistent with a simple extrapolation of the low temperature rate constants according to the crossing-point model of Bates and Massey for atom-atom ionizing collisions.

UNCLASSIFIED

1. Shock Waves - Electron Density.
2. Air, Ionized.
3. Air, Dissociated.
4. Electron Density - Measurement.
5. Shock Waves - Ionization.
I. Title.
II. Lin, S. C.
III. Teare, J. D.
IV. Avco-Everett Research Report 115.
V. AFCRL - 62 - 751.
VI. Contract AF 19(604) - 7458.

UNCLASSIFIED

UNCLASSIFIED

Avco-Everett Research Laboratory, Everett, Massachusetts
RATE OF IONIZATION BEHIND SHOCK WAVES IN AIR - II. THEORETICAL INTERPRETATION, by S. C. Lin and J. D. Teare. September 1962. 67 p. incl. illus. (Project 5561; Task 46308) (Avco-Everett Research Report 115; AFCRL - 62 - 751)
(Contract AF 19(604) - 7458)
Unclassified report

The problem of spontaneous ionization (i. e., no externally applied electromagnetic fields, nor hard radiation) in the reaction zone behind strong normal sbock waves in air has been treated concurrently with the problem of dissociarion and vibrational relaxation. Through a comparison of specific ionization rates, one may conclude that up to a shock velocity of 10 km/sec (about 30 times the speed of sound at room temperature) the predominant electron production process would be atom-atom ionizing collisions. This would be followed in an approximately decreasing order of impottance by photo-ionization, electron impact, atom-molecule collisions and

(over)

molecule-molecule collisions. The charge exchange reactions, while not contributing directly to the electron production process, were found to have a small but noticeable indirect effect on the resultant electron density distribution at some distance behind the shock due to their continuous shifting of the relative population between atomic and molecular ions (which recombine with the electrons at different rates). The specific rate constants for the atom-atom processes required to interpret all existing experimental results appear to be consistent with a simple extrapolation of the low temperature rate constants according to the crossing-point model of Bates and Massey for atom-atom ionizing collisions.

UNCLASSIFIED

1. Shock Waves - Electron Density.
2. Air, Ionized.
3. Air, Dissociated.
4. Electron Density - Measurement.
5. Shock Waves - Ionization.
I. Title.
II. Lin, S. C.
III. Teare, J. D.
IV. Avco-Everett Research Report 115.
V. AFCRL - 62 - 751.
VI. Contract AF 19(604) - 7458.

UNCLASSIFIED

UNCLASSIFIED

UNCLASSIFIED

Avco-Everett Research Laboratory, Everett, Massachusetts
RATE OF IONIZATION BEHIND SHOCK WAVES IN AIR - II. THEORETICAL INTERPRETATION, by S. C. Lin and J. D. Teare. September 1962. 67 p. incl. illus. (Project 5561; Task 46308) (Avco-Everett Research Report 115; AFCRL-62-751)
(Contract AF 19(604)-7458)

Unclassified report

The problem of spontaneous ionization (i. e., no externally applied electromagnetic fields, nor hard radiation) in the reaction zone behind strong normal shock waves in air has been treated concurrently with the problem of dissociation and vibrational relaxation. Through a comparison of specific ionization rates, one may conclude that up to a shock velocity of 10 km/sec (about 30 times the speed of sound at room temperature) the predominant electron production process would be atom-atom ionizing collisions. This would be followed in an approximately decreasing order of importance by photo-ionization, electron impact, atom-molecule collisions and

(over)

UNCLASSIFIED

1. Shock Waves - Electron Density.
2. Air, Ionized.
3. Air, Dissociated.
4. Electron Density - Measurement.
5. Shock Waves - Ionization.
I. Title.
II. Lin, S. C.
III. Teare, J. D.
IV. Avco-Everett Research Report 115.
V. AFCRL-62-751.
VI. Contract AF 19(604)-7458.

UNCLASSIFIED

Avco-Everett Research Laboratory, Everett, Massachusetts
RATE OF IONIZATION BEHIND SHOCK WAVES IN AIR - II. THEORETICAL INTERPRETATION, by S. C. Lin and J. D. Teare. September 1962. 67 p. incl. illus. (Project 5561; Task 46308) (Avco-Everett Research Report 115; AFCRL-62-751)
(Contract AF 19(604)-7458)

Unclassified report

The problem of spontaneous ionization (i. e., no externally applied electromagnetic fields, nor hard radiation) in the reaction zone behind strong normal shock waves in air has been treated concurrently with the problem of dissociation and vibrational relaxation. Through a comparison of specific ionization rates, one may conclude that up to a shock velocity of 10 km/sec (about 30 times the speed of sound at room temperature) the predominant electron production process would be atom-atom ionizing collisions. This would be followed in an approximately decreasing order of importance by photo-ionization, electron impact, atom-molecule collisions and

(over)

UNCLASSIFIED

1. Shock Waves - Electron Density.
2. Air, Ionized.
3. Air, Dissociated.
4. Electron Density - Measurement.
5. Shock Waves - Ionization.
I. Title.
II. Lin, S. C.
III. Teare, J. D.
IV. Avco-Everett Research Report 115.
V. AFCRL-62-751.
VI. Contract AF 19(604)-7458.

UNCLASSIFIED

molecule-molecule collisions. The charge exchange reactions, while not contributing directly to the electron production process, were found to have a small but noticeable indirect effect on the resultant electron density distribution at some distance behind the shock due to their continuous shifting of the relative population between atomic and molecular ions (which recombine with the electrons at different rates). The specific rate constants for the atom-atom processes required to interpret all existing experimental results appear to be consistent with a simple extrapolation of the low temperature rate constants according to the crossing-point model of Bates and Massey for atom-atom ionizing collisions.

UNCLASSIFIED

molecule-molecule collisions. The charge exchange reactions, while not contributing directly to the electron production process, were found to have a small but noticeable indirect effect on the resultant electron density distribution at some distance behind the shock due to their continuous shifting of the relative population between atomic and molecular ions (which recombine with the electrons at different rates). The specific rate constants for the atom-atom processes required to interpret all existing experimental results appear to be consistent with a simple extrapolation of the low temperature rate constants according to the crossing-point model of Bates and Massey for atom-atom ionizing collisions.

UNCLASSIFIED

Avco-Everett Research Laboratoty, Everett, Massachusetts
RATE OF IONIZATION BEHIND SHOCK WAVES IN AIR - II. THEORETICAL INTERPRETATION, by S. C. Lin and J. D. Teare. September 1962. 67 p. incl. illus. (Project 5561; Task 46308) (Avco-Everett Research Report 115; AFCRL - 62 - 751)
(Contract AF 19(604) - 7458)
Unclassified report

Tbe problem of spontaneous ionization (i. e., no externally applied electromagnetic fields, nor hard radiation) in the reaction zone behind strong normal shock waves in air has been treated concurrently with the ptoblem of dissociation and vibrational relaxation. Through a comparison of specific ionization rates, one may conclude that up to a shock velocity of 10 km/sec (about 30 times the speed of sound at room temperature) the predominant electron production process would be atom-atom ionizing collisions. This would be followed in an approximately decreasing order of importance by photo-ionizatinn, electron impact, atom-molecule collisions and

(over)

molecule-molecule collisions. The charge exchange reactions, while not contributing directly to the electron production process, were found to have a small but noticeable indirect effect nn the resultant electron density distribution at some distance behind the shock due to their continuous shifting of the relative population between atomic and molecular ions (which recombine with the electrons at different rates). The specific rate constants fnr the atnm-atom processes required to interpret all existing experimental results appear to be cnnsistent with a simple extrapolation of the low temperature rate constants according to the ctossing-point model of Bates and Massey for atom-atom ionizing collisions.

UNCLASSIFIED

1. Shock Waves - Electron Density.
2. Air, Ionized.
3. Air, Dissociated.
4. Electron Density - Measurement.
5. Shock Waves - Ionization.
I. Title.
II. Lin, S. C.
III. Teare, J. D.
IV. Avco-Everett Researcb Report 115.
V. AFCRL - 62 - 751.
VI. Contract AF 19(604) - 7458.

UNCLASSIFIED

UNCLASSIFIED

Avco-Everett Research Laboratory, Everett, Massacbusetts
RATE OF IONIZATION BEHIND SHOCK WAVES IN AIR - II. THEORETICAL INTERPRETATION, by S. C. Lin and J. D. Teare. September 1962. 67 p. incl. illus. (Project 5561; Task 46308) (Avco-Everett Research Report 115; AFCRL - 62 - 751)
(Contract AF 19(604) - 7458)
Unclassified report

The problem of spontaneous ionization (i. e., no externally applied electromagnetic fields, nor hard radiation) in the reaction zone behind strong normal shock waves in air bas been treated concurrently with the ptoblem of dissnciation and vibrational relaxation. Through a comparison of specific ionization rates, one may conclude that up to a shock velocity of 10 km/sec (about 30 times the speed of sound at room temperature) the predominant electron production process would be atom-atom ionizing collisions. This would be followed in an approximately decreasing order of importance by photo-ionization, electron impact, atom-molecule collisions and

(over)

molecule-molecule collisions. The charge exchange reactions, while not contributing directly to the electron production process, were found to bave a small but noticeable indirect effect on the resultant electron density distribution at some distance behind the shnck due tn their continunus shifting of the relative population between atomic and molecular ions (which recombine with the electrons at different rates). The specific rate constants for the atom-atom processes required to interpret all existing experimental results appear to be consistent with a simple extrapolation of tbe low temperature rate constants according to the crossing-point model of Bates and Massey fnr atom-atom ionizing collisions.

UNCLASSIFIED

1. Shock Waves - Electron Density.
2. Air, Ionized.
3. Air, Dissociated.
4. Electron Densi... - Measurement.
5. Shock Waves - Ionization.
I. Title.
II. Lin, S. C.
III. Teare, J. D.
IV. Avco-Everett Researcb Report 115.
V. AFCRL - 62 - 751.
VI. Contract AF 19(604) - 7458.

UNCLASSIFIED

UNCLASSIFIED

UNCLASSIFIED

Avco-Everett Research Laboratory, Everett, Massachusetts
RATE OF IONIZATION BEHIND SHOCK WAVES IN AIR - II. THEORETICAL INTERPRETATION, by S. C. Lin and J. D. Teare. September 1962. 67 p. incl. illus. (Project 5561; Task 46308) (Avco-Everett Research Report 115; AFCRL-62-751)
(Contract AF 19(604)-7458)

Unclassified report

The problem of spontaneous ionization (i. e., no externally applied electromagnetic fields, nor hard radiation) in the reaction zone behind strong normal shock waves in air has been treated concurrently with the problem of dissociation and vibrational relaxation. Through a comparison of specific ionization rates, one may conclude that up to a shock velocity of 10 km/sec (about 30 times the speed of sound at room temperature) the predominant electron production process would be atom-atom ionizing collisions. This would be followed in an approximately decreasing order of impottance by photo-ionization, electron impact, atom-molecule collisions and

(over)

molecule-molecule collisions. The charge exchange reactions, while not contributing directly to the electron production process, were found to have a small but noticeable indirect effect on the resultant electron density distribution at some distance behind the shock due to their continuous shifting of the relative population between atomic and molecular ions (which recombine with the electrons at different rates). The specific rate constants for the atom-atom processes required to interpret all existing experimental results appear to be consistent with a simple extrapolation of the low temperature rate constants according to the crossing-point model of Bates and Massey for atom-atom ionizing collisions.

UNCLASSIFIED

1. Shock Waves - Electron Density.
2. Air, Ionized.
3. Air, Dissociated.
4. Electron Density - Measurement.
5. Shock Waves - Ionization.

I. Title.
II. Lin, S. C.
III. Teare, J. D.
IV. Avco-Everett Research Report 115.
V. AFCRL-62-751.
VI. Contract AF 19(604)-7458.

UNCLASSIFIED

UNCLASSIFIED

UNCLASSIFIED

Avco-Everett Research Laboratory, Everett, Massachusetts
RATE OF IONIZATION BEHIND SHOCK WAVES IN AIR - II. THEORETICAL INTERPRETATION, by S. C. Lin and J. D. Teare. September 1962. 67 p. incl. illus. (Project 5561; Task 46308) (Avco-Everett Research Report 115; AFCRL-62-751)
(Conrract AF 19(604)-7458)

Unclassified report

The problem of spontaneous ionization (i. e., no externally applied electromagnetic fields, nor hard radiation) in the reaction zone behind strong normal shock waves in air has been treated concurrently with the problem of dissociation and vibrational relaxation. Through a comparison of specific ionization rates, one may conclude that up to a shock velocity of 10 km/sec (about 30 times the speed of sound at room temperature) the predominant electron production process would be atom-atom ionizing collisions. This would be followed in an approximately decreasing order of importance by photo-ionization, electron impact, atom-molecule collisions and

(over)

molecule-molecule collisions. The charge exchange reactions, while not contributing directly to the electron production process, were found to have a small but noticeable indirect effect on the resultant electron density distribution at some distance behind the shock due to their continuous shifting of the relative population between atomic and molecular ions (which recombine with the electrons at different rates). The specific rate constants for the atom-atom processes required to interpret all existing experimental results appear to be consistent with a simple extrapolation of the low temperature rare constants according to the crossing-point model of Bates and Massey for atom-atom ionizing collisions.

UNCLASSIFIED

1. Shock Waves - Electron Density.
2. Air, Ionized.
3. Air, Dissociated.
4. Electron Density - Measurement.
5. Shock Waves - Ionization.

I. Title.
II. Lin, S. C.
III. Teare, J. D.
IV. Avco-Everett Research Report 115.
V. AFCRL-62-751.
VI. Contract AF 19(604)-7458.

UNCLASSIFIED

UNCLASSIFIED